ABSTRACT BOOK

3rd Conference on

Image-Guided Interventions & Fokus Neuroradiologie

RECENT PROGRESS AND DEVELOPMENTS

November 6 and 7, 2017 Magdeburg, Germany

Conference Chairs

Prof. Dr. Martin Skalej
Otto-von-Guericke-Universität Magdeburg
Institut für Neuroradiologie
Leipziger Str. 44
39120 Magdeburg, Germany

Prof. Dr. Christoph Hoeschen
Otto-von-Guericke-Universität Magdeburg
Institut für Medizintechnik (IMT)
Universitätsplatz 2, Gebäude 09
39016 Magdeburg, Germany

Organizer

Otto-von-Guericke-Universität Magdeburg
Universitätsklinikum A.ö.R.
Institut für Neuroradiologie
Magdeburg, Germany

Medizinische Hochschule Hannover
Institut für Diagnostische und
Interventionelle Neuroradiologie
Hannover, Germany

Forschungscampus STIMULATE
Magdeburg, Germany

Forschungscampus M²OLIE
Mannheim, Germany

Index

Actual molecular diagnostic methods for interventions

ID 31

3D tumor cell models for the analysis of radiotheranostics

J. Klicks[1], R. Rudolf[1], M. Hafner[1]
[1]Institut für Molekular- und Zellbiologie, Hochschule Mannheim, Mannheim, Germany

Introduction: We established 2D- and 3D-cell culture protocols, including spheroid and perfusion-based culture systems. Keratinocytes (HaCaT), melanoma (SK-MEL-28), and prostate cancer cells (LNCaP, PC-3), have been used to establish 3D tumor cell models for the analysis of radiotheranostics distribution and function.
Materials & methods: 3D-cultures were grown as spheroids in 96 well plates with cell-repellent surfaces or on a perfusable chip-based bioreactor system.
Results: HaCaT, SK-MEL-28, LNCaP and PC-3 cells formed spheroids on cell-repellent plates. PC-3 cells needed the addition of Matrigel to form spheroids. While cancer spheroids were increasing in size over time, HaCaT spheroids were shrinking. In 2D, HaCaT, SK-MEL-28, LNCaP, and PC-3 cells were strongly proliferating. Conversely, in a spheroid, HaCaT cells were not proliferating anymore and SK-MEL-28 spheroids show only proliferation in the periphery. On the KITChip, HaCaT cells were hardly proliferating, while SK-MEL-28 cells displayed proliferation on the outside of the 3D structure. LNCaP spheroids showed only sparse proliferation and PC-3 spheroids were proliferating peripherally. In 2D, HaCaT, SK-MEL-28, LNCaP, and PC-3 cells showed no apoptotic cells. When grown as spheroid or on the KITChip, HaCaT cells presented irregular distribution of apoptosis. SK-MEL-28 spheroids displayed almost no apoptosis while on the KITChip there were a few apoptotic cells. In spheroid culture, LNCaP and PC-3 cells were apoptotic predominantly in the center.
Conclusion: 3D models were established for the study of theranostics against different tumor entities, including melanoma and prostate. Phenotypic analysis methods were developed.

ID 46

Efficient modification of GRPR-specific gold nanoparticles for fluorescence imaging of prostate carcinoma

M. Pretze[1], A. Hien[2], M. Roscher[1], K. Richter[3], M. Rädle[2]
S. Litau[1], C. Wängler[4], B. Wängler[1]
[1]Department of Clinical Radiology and Nuclear Medicine, Medical Faculty Mannheim of Heidelberg University, University Medical Cen, Molecular Imaging & Radiochemistry , Mannheim, Germany
[2]Mannheim University of Applied Sciences, Institute of Process Control and Innovative Energy Conversion , Mannheim, Germany
[3]German Cancer Research Center (DKFZ), Central Unit Electron Microscopy / W230 , Heidelberg, Germany
[4]Department of Clinical Radiology and Nuclear Medicine, Medical Faculty Mannheim of Heidelberg University, University Medical Center Mannheim, Biomedical Chemistry , Mannheim, Germany

Introduction: The focus of this work was on the development of bimodal contrast agents based on gold nanoparticles (AuNP) which allow a custom surface-modification[1]. By simple ligand exchange it is possible to introduce chemoselectively reacting functionalities suitable for complementary particle functionalization. E.g., we introduced near-infrared (NIR) dyes for fluorescence imaging and Bombesin$_{(7\text{-}14)}$ (BBN$_{(7\text{-}14)}$) as exemplary targeting vector which addresses GRP-receptors often overexpressed on the surface of prostate carcinoma.
Materials & methods: The AuNP were synthesized by the method of Brust and Schiffrin and labeled with thiol-functionalized ligands[1]. The characterization of the AuNP was performed by NMR, TEM, UV/Vis and TGA. To evaluate the cell uptake of the functionalized AuNP in GRPR expressing cells, *in vitro* experiments were performed using PC3-(GRPR-positive) and A431-(GRPR-negative) cells. Furthermore, the AuNP were tested for their fluorescence imaging properties *in vitro* in cells and *in vivo* at healthy SHO mice and PC3 tumor-bearing mice. The AuNP **4** were also tested at a newly developed optical tomograph for live fluorescence imaging.
Results: The avidity of the BBN$_{(7\text{-}14)}$-modified AuNP **4** towards the GRPR was found to be much lower compared to monomeric BBN$_{(7\text{-}14)}$ (IC$_{50}$ **4** = 2.91 nM, IC$_{50}$ BBN$_{(7\text{-}14)}$ = 60.27 nM). Via confocal fluorescence microscopy, the cell internalization of the particles was verified. The cellular uptake of the dually modified particles could partly be blocked by BBN$_{(7\text{-}14)}$. The animal experiments revealed a higher accumulation of **4** in PC3-tumor in comparison to muscle at 24 h post i.v. injection.
Conclusion: These initial results show that the dually modified particles show potential as bimodal imaging tools for GRPR-expressing tumors *in vivo* via CT as well as optical imaging during surgery.

Scheme 1. Syntheses pathway for GRPR-specific, fluorescent AuNP **4**.

[1] J. Zhu, C. Waengler, et al. Langmuir 2012, 28, 5508.

Figure 1

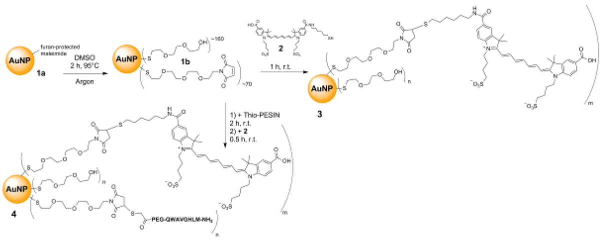

Aneurysms

ID 06

Virtual enhancement of marker X-ray visibility for cerebral stents and flow diverters

S. Manthey[1], T. Hoffmann[2], G. Cattaneo[3], O. Beuing[2]
B. Preim[1], S. Saalfeld[1]

[1] Otto-von-Guericke-University, Department of Simulation and Graphics, Magdeburg, Germany

[2] Otto-von-Guericke-University, Institute of Neuroradiology, Magdeburg, Germany

[3]Acandis GmbH, Pforzheim, Germany

Introduction: Stents are common devices for endovascular X-ray-guided treatment of neurovascular diseases like aneurysms or artherosclerosis, but their visibility may be hampered in clinical practice. To improve visibility during interventions, they are equipped with radiopaque markers. However, since the marker size is limited, stents may still be nearly invisible during deployment. Therefore, we virtually enhanced these markers with an overlay supplied by a detection algorithm.

Materials & methods: For marker location, we used a feature detector according to their appearance in fluoroscopy and radiographic images. To increase perceptibility in regions with dense bone, we first subtracted a reference frame from the current frame. False positives detection results were eliminated through post-processing. After detection, marker locations were visually enhanced with an overlay (see Fig. 1). For validation, eight data sets were acquired with a skull phantom and different stents in an angio lab. Subsequently, a physician compared the enhanced and the unaltered images qualitatively. In order to examine the characteristics of the proposed method further we supplied a confusion matrix and investigated the sensitivity and specificity of our method.

Results: An overlay was created in all cases. In regions where bone masked the markers in fluoroscopy, the subtraction of a reference frame allowed their detection. The improved images support physicians to discern devices. In addition, our method was tested on clinical data with promising results.

Conclusion: The proposed approach successfully demonstrates that the visibility of stent markers can be increased with image-based techniques and that markers of current devices are of sufficient size and opacity to be detected by low level feature detectors. In future, the image-based detection of X-Ray markers may assist in precise stent deployment in difficult interventions and create new possibilities for the design of X-Ray markers.

Figure 1

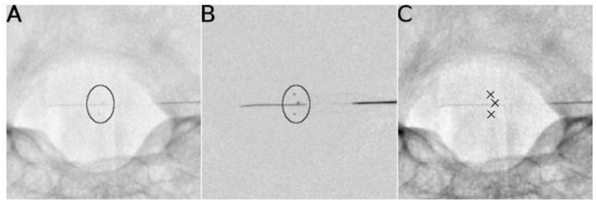

Figure 1: A: Section of an original image with stent marker indicated by the black ellipse and guide wire, B: Same section after subtraction of reference image with stent marker indicated by the black ellipse, C: section with detected markers indicated by symbols

ID 18

Automatic Viewpoint Selection for Exploration of Time-dependent Cerebral Aneurysm Data

M. Meuschke[1,2], O. Beuing[2,3], B. Preim[1,2], K. Lawonn[4]

[1]Otto-von-Guericke Universität, Department of Simulation and Graphics , Magdeburg, Germany

[2]STIMULATE, Magdeburg, Germany

[3]Institute of Neuroradiology, University Hospital of Magdeburg, Magdeburg, Germany

[4]University of Koblenz-Landau, Institute for Computational Visualistics, Koblenz, Germany

Question: For the rupture risk evaluation of cerebral aneurysms, a combined investigation of morphological and hemodynamic data is necessary. However, the extensive nature of the time-dependent data complicates the analysis. Domain experts have to manually determine appropriate views, which can be a tedious and time-consuming process.

Methods: We present an automatic selection of viewpoints, forming a camera path, to support the exploration of simulated aneurysm data based on scalar input data such as wall thickness or pressure. The viewpoint selection is modeled as an optimization problem. For each time step, a set of optimal viewpoints is calculated. We order these viewpoints and connect them to a camera path. Moreover, the viewpoints are combined between adjacent time steps to generate a global camera animation during the cardiac cycle.

Results: We calculated camera animations for five data sets and evaluated the results with two domain experts, which assess if the camera path supports the time-dependent data exploration. Moreover, they had to manually search for suspicious surface regions depending on selected parameters. The experts described the camera path as very helpful for the exploration. The selected views correlated with the manual results within that time step. However, for the manual searching a series of rotations was necessary. Moreover, the experts liked that no further specification of thresholds is necessary for the calculation.

Conclusion: Our domain experts confirmed the importance of camera paths to support the data exploration. A possible application of our method is to get a quick overview of the aneurysm data, where rupture-prone areas are presented. In addition, it could support the clinical report generation and serve as a summary of a patient's rupture risk. In the future, we want to integrate information about specific blood flow patterns to select views that present the time-dependent vortex behavior.

ID 19

Impact of stent-induced vessel deformation on the hemodynamic of intracranial aneurysms

S. Voß[1], P. Berg[1], G. Janiga[1], O. Beuing[2]
[1]University of Magdeburg "Otto von Guericke", Lab. of Fluid Dynamics & Technical Flows, Magdeburg, Germany
[2]University Hospital Magdeburg, Institute of Neuroradiology, Magdeburg, Germany

Stent-assistend coiling therapy has become an important and succesful treatment routine for intracranial aneurysms. Observation in clinical practice showed that such interventions can lead to a deformation of the vessel or aneurysm shape due to the stiffness of the stent. Especially regarding middle cerebral and anterior communicating arteries this is a common but unwanted side effect.

In this study, pre- and post-interventional 3D rotational angiography image data is evaluated. In order to quantify the impact of the vessel wall deformation on the intra-aneurysmal hemodynamics, eight virtual configurations are genereated varying a) the deformation state, b) the presence of a stent, and c) the presence of coils. Therefore, stents and coils are virtually implanted into the segmented image data. Further, flow simulations of the different configurations were carried out using Computational Fluid Dynamics.

The hemodynamic simulations reveal distinct differences in intra-aneurysmal flow velocities, the aneurysm neck inflow rate, local wall shear stresses, the oscillatory shear index, and the relative residence time. This leads to two main findings: 1) The stent-induced vessel wall deformation itself can exceed the therapeutic effect of the coils, and 2) The deformation can reinforce as well as impair the coil embolization.

This study suggests to consider possible vessel wall deformations in the stent-assisted coiling therapy for middle cerebral artery aneurysms. Further, a targeted modification of the vessel shape redirecting the blood flow to minimize the amount of blood entering the aneurysm may be useful as a novel tool for treatment planning.

ID 29

A semi-automatic simulation environment for the identification of a patient-specific aneurysm treatment

P. Berg[1], L. Daróczy[1], G. Janiga[1], O. Beuing[2]
[1]University of Magdeburg, Department of Fluid Dynamics, Magdeburg, Germany
[2]University of Magdeburg, Institute of Neuroradiology, Magdeburg, Germany

Endovascular treatment of intracranial aneurysms is a promising therapy option compared to invasive techniques. Especially flow-diverter stents drastically reduce the entering blood flow promoting thrombotic occlusions. However, deployment difficulties as well as post-operative complications are reported that limit the usability of flow-diverting devices.

To improve the individual treatment outcome of a patient, hemodynamic simulations before and after virtual stenting are carried out. In this regard, different virtual stent configurations with varying stent strut numbers, wire diameters and pore angles are considered to identify the optimal treatment strategy for a patient-specific aneurysm. In the recent study, one case was chosen as a proof-of-concept, considering over 100 different stent designs.

The simulation results demonstrate a strong variety of possible intervention scenarios. Hence, for a given flow-diverter porosity an optimized stent geometry is identified that maximizes the blood flow reduction into the dilatation. Additionally, wall shear stresses are significantly reduced for improved stent designs, whereas the analyses of any arbitrary hemodynamic parameter can be included into the automatized workflow.

The virtual stenting method enables the attending physician to carefully select an appropriate flow-diverter device that fulfills the requirements of an individual patient. Furthermore, due to highly efficient optimization algorithms as well as a strong parallelization of the computations, simulation times that are clinically reasonable can be achieved.

Modeling and information technology in imaging

ID 04

Visualization of Robotic Trajectories from CT Image Data

N. Merten[1], S. Saalfeld[1], B. Preim[1]

[1]University of Magdeburg, Department of Simulation and Graphics, Magdeburg, Germany

Question: One possibility to use robotic assistance during Radiofrequency Ablations is a hand-guided approach where a physician and robot insert instruments cooperatively. The instruments' trajectories are defined during intervention planning. This can be done by drawing a line in a medical image stack, while interpreting the line as an ordered list of coordinate points. In this work we want to describe and compare two methods to visualize trajectories directly when Computed Tomography images are used.
Methods: For the first method, the line's coordinates are discretized to integer-valued sample points with the Bresenham algorithm. For the second method, the line is divided into equidistant sample points and the resulting value is trilinearly interpolated from neighboring voxel values. The resulting sample values can then be visualized as a graph curve.
Results: Our preliminary results are presented in Figure 1: The left subfigure shows a volume rendered data set and an orange line. This line leads from outside the body into a lower thoracic vertebra. The right subfigure shows our results when we used the aforementioned methods. The resulting graphs can be interpreted as follows: While the instrument's current position is used as a point of refererence, the slopes indicate at which line sections the robot's operator can expect less (downward slope), the same (roughly constant graph), or more (upward slope) resistance.
Conclusion: We described two methods to create direct trajectory visualizations for instruments in CT scans. One benefit of our visualization is that it depicts the density distribution along planned trajectories. Additionally, the operator can easily see when changes in resistance can be expected when instruments are inserted with robotic assistance.
Figure 1: On the **left**, we defined an exemplary trajectory into a lower thoracic vertebra. The ***right*** subfigure shows the result for both methods and the instrument's current position during insertion.

Figure 1

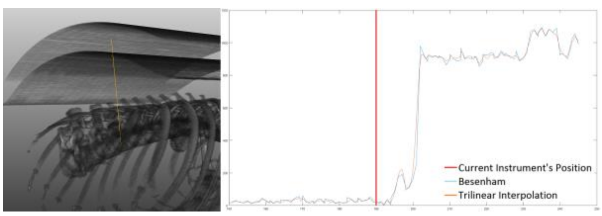

ID 05

Image similarity metric evaluation for multimodal registration of the liver

B. Trimborn[1,2], A. Ilina[3,2], S. Engelhardt[1,4], F. Zöllner[2]
L. Schad[2], I. Wolf[1]

[1]Mannheim University of Applied Sciences, Institute for Medical Informatics, Mannheim, Germany

[2]Heidelberg University, Medical Faculty Mannheim, Computer Assisted Clinical Medicine, Mannheim, Germany

[3]Queen's University, Laboratory for Percutaneous Surgery, Kingston, Canada

[4]Heidelberg University, Department of Cardiac Surgery, Heidelberg, Germany

Multimodal image registration benefits image-guided procedures by providing complementary information for surgical planning or treatment monitoring. There exists a variety of registration methods that show a significant difference in performance depending on the underlying data. Hence, we conducted a comparative study of similarity metrics, such as Advanced Mattes Mutual Information (AMMI), Normalized Correlation (NC) and Normalized Mutual Information (NMI), for the registration of multimodal liver scans.
Data sets of three patients, including T1- and T2-weighted MRI and intra-interventional Cone-Beam CT (CBCT) data, were manually registered to conventional CT data by setting 16 reference points to create a ground truth for the registration evaluation. To determine the registration accuracy after applying translation transformations in a range from 5-30mm, equally spaced points were created inside the liver serving as landmarks for the estimation of the target registration error (TRE) before and after registration. The registration performance was evaluated for the registration of CBCT, T1 and T2 to CT and T2 to T1.
For the registration of CBCT to CT, all metrics achieved similar TRE after registration with the metrics relying on MI slightly outperforming the NC metric (Fig.1). Notably, the NC metric – usually considered to be applicable to monomodal applications only – also achieved similar results for the multimodal registration of T1 to CT with a capture range of at least 25 mm (threshold 5 mm). For the registration of T2 to CT and T2 to T1, MI-based methods yielded a lower TRE than NC as expected.
This performance comparison of standard similarity metrics showed that, for the specific case of liver scans, NC is able to compete with MI-based methods in terms of registration accuracy for the multimodal registration of T1 to CT which may be attributed to a correlated grey value distribution in the liver and immediate surrounding tissue in both modalities.

Figure 1

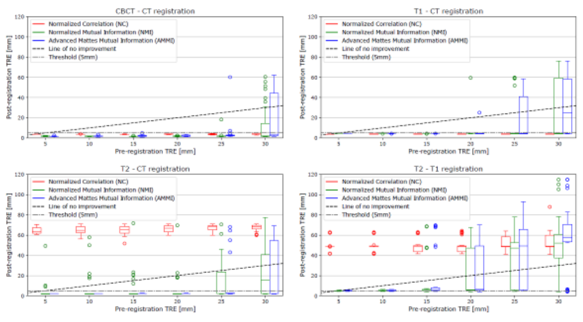

Fig.1: Results obtained for the registration of CBCT to CT, T1 MRI to CT, T2 MRI to CT and T2 to T1 MRI for one of the three patients.

ID 07

A multi-modal multi-compartment perfusion phantom for microvascular tracer kinetic modelling

T. Gaa[1], L. Schad[1], F. Zöllner[1]

[1]Computer Assisted Clinical Medicine, Medical Faculty Mannheim, Heidelberg University, Mannheim, Germany

Dynamic contrast enhanced (DCE)-MRI and CT combined with tracer kinetic modelling allows for the determination of quantitative perfusion parameters. To investigate their reproducibility by imitating tissue on a capillary level we propose to use a dialysis filter that has a semipermeable capillary membrane which can be crossed by MR and CT-contrast agent (CA). This way, a dual-compartment model that depicts anatomical conditions more accurately can be realized.

A dialysis filter was used to imitate tissue characteristics with fibers close to the capillary size. The transfer of CA through a semipermeable membrane from within the fibers to the surrounding space was tested. Water and automatically injected CA were pumped through the phantom with typical blood flow velocities. A tube in front of the phantom inlet served as an artificial artery where the first pass of CA signal was measured and used to determine the (arterial) input function (AIF). Dynamic imaging was performed at a 3T MRI and CT scanner to enable calculation of perfusion parameters.

The measured signal shows the transfer of CA from the fibers into the surrounding space and subsequent wash-out by the dialysate circuit. The wash-out process follows a typical clearance function. The phantom generates AIFs and tissue functions with characteristic first pass and typical wash-out slope for all tested flow velocities. For lower velocities, curves start with a delay compared to higher velocities and exhibit a broader distribution.

The initial findings of this study show that the perfusion phantom may serve as a tissue mimicking device, able to produce typical signal curves for both AIF and tissue function in CT and MRI. The semipermeable membrane of the fibers enables the simulation of two-compartment kinetics imitating capillaries and interstitium as found in the human body. Quantitative perfusion parameters can be determined and may provide additional information about extravasation at phantom capillaries.

Figure 1

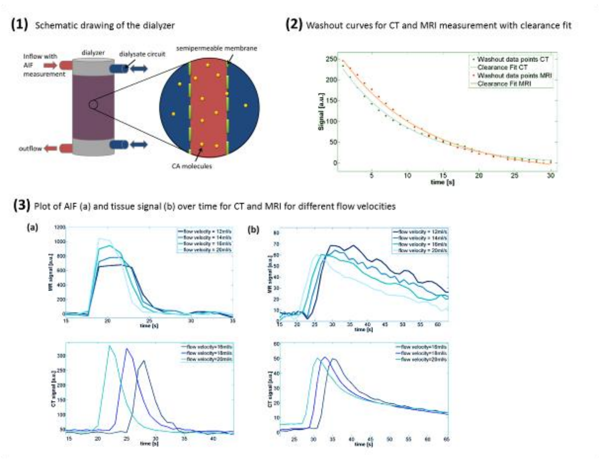

ID 09

Streak Artifact Reduction in Limited Angle Tomography Using Machine Learning

Y. Huang[1], Y. Lu[1], O. Taubmann[1,2], G. Lauritsch[1]
A. Maier[1,2]

[1]Friedrich-Alexander-University Erlangen-Nuremberg, Pattern Recognition Lab, Erlangen, Germany

[2]Erlangen Graduate School in Advanced Optical Technologies (SAOT), Erlangen, Germany

Question: In limited angle tomography, streak artifacts occur due to missing data. They may cause wrong decisions in clinical applications. Therefore, streak artifact reduction has important clinical value. In this work, three machine learning techniques, namely linear regression (LR), multi-layer perception (MLP), and reduced-error pruning tree (REPTree), are investigated to predict streak artifacts.

Methods: The input observations are the images reconstructed from the limited angle data. The output labels are the residual artifact images. The mapping of an image patch to a single output value for the center pixel of that patch is learned.

Regarding feature extraction, for each pixel in the input images, we choose its intensity and the mean, variance, and median statistic of the image patch which we call MVM features. Since the streak artifacts have specific orientations, the two eigenvalues and the orientation of the main eigenvector of the Hessian matrix at each pixel are chosen as well.

LR, MLP, and REPTree are evaluated on simulated data generated from the Shepp-Logan phantom and CT images in both parallel-beam and fan-beam. For the Shepp-Logan data, we pick 150 slices from the 3-D volume and one half of them are used for training, the other half for testing. For the CT data, we use 7 patients for training and another 7 patients for testing.

Results: The results on the Shepp-Logan data demonstrate that REPTree predicts streak artifacts best (Fig. 1). REPTree also reduces streak artifacts well for the CT data in parallel-beam (Fig. 2). In fan-beam, streaks are reduced as well, even though some artifacts are introduced by misclassification (Fig. 3).

Conclusions: When using the MVM and Hessian features, REPTree classifies streak artifacts better than LR and MLP and shows potential for clinical applications.

Disclaimer: The concepts and information presented in this paper are based on research and are not commercially available.

Figure 1

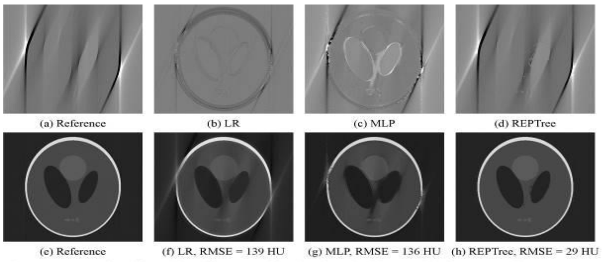

Fig. 1. Learnt streak artifacts using different machine learning algorithms and their corresponding reconstruction images in parallel-beam with a 160° angular range. The root-mean-square errors (RMSE) of images learnt by LR, MLP, and REPTree are shown in subtitles of (f)-(h). Window width for the top row: 1200 HU; window for the bottom row: [-1400, 1400] HU.

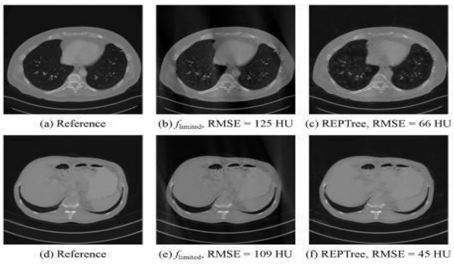

Fig. 2. The reference images, the 160° limited angle reconstructions ($f_{limited}$), and the machine learning results using REPTree of the low-dose CT data in parallel-beam geometry. Window: [-1150, 1300] HU.

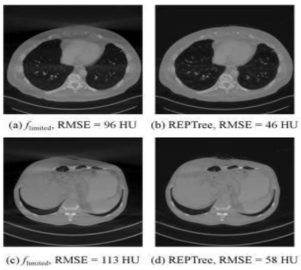

Fig. 3. The 170° limited angle reconstructions ($f_{limited}$) and the machine learning results using REPTree of the low-dose CT data in fan-beam geometry. Window: [-1150, 1300] HU.

ID 10

GPU-accelerated simulation of radiofrequency ablation of spine metastasis.

C. Rieder[1], M. Becker[2], S. Serowy[2], H. Ballhausen[1]
C. Schumann[1], M. Skalej[2]
[1]Fraunhofer MEVIS, Bremen, Germany
[2]Universitätsklinikum Magdeburg, Institut für Neuroradiologie, Magdeburg, Germany

Introduction: Radiofrequency ablation (RFA) is a procedure option for the palliative treatment of painful spinal metastasis based on local tissue heating. The goal is the complete coagulation of the metastases. Therefore, needle positions and ablation parameters have to be chosen in order to achieve complete ablation without harming risk structures (e.g. spinal cord). In this work, we present a numerical simulation method to predict the induced heat and compare results against the outcome of real ablations.

Materials and Methods: The developed numerical simulation method allows to compute the temperature distribution over time based on the generator protocol, from which an Arrhenius damage image is computed. The numerical solver is massively parallelized and implemented on the graphics processing unit (GPU) allowing for fast calculations in less than 15 seconds on a standard computer. The method has been integrated into the SAFIR platform. To demonstrate the value of our method, numerical simulations have been retrospectively compared with 31 post-ablative necroses from 28 patients. Therefore, metastasis, vertebra, and spinal cord have been segmented from pre-interventional MR images. Intra-interventional Cone Beam CT images have been registered for the placement of RF needles. Finally, the coagulation necroses have been segmented from post-interventional MR images and have been registered with pre-interventional images.

Results: After computation of the numerical simulations considering the documented ablation parameters, the damage images are statistical compared with the necroses in 3D according to shape, volume, and size. On average, a DICE coefficient of 0.58, a volumetric overlap of 0.42, and a mean surface distance of 3.92 mm as well as a sensitivity of 77% and a positive predictive value of 54% are measured.

Conclusions: We have demonstrated that the proposed method has the potential to predict the expected thermal damage before the ablation procedure.

Figure 1

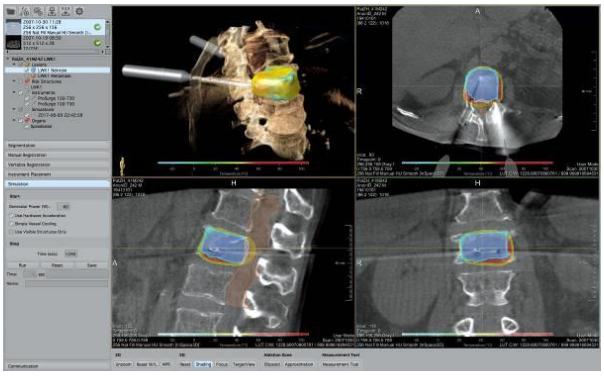

ID 20

A fast numerical simulation library for thermal ablation procedures

J. Georgii[1], T. Pätz[1], C. Rieder[1], T. Preusser[1,2]
[1]Fraunhofer MEVIS, Bremen, Germany
[2]Jacobs University Bremen, Bremen, Germany

Introduction: We present a numerical simulation library for treatment planning of hyperthermia and ablation procedures taking patient-specific anatomy into account. The library is able to simulate radiofrequency (RF), microwave (MW), laser, and cryo interventions and has been integrated into a planning software.

Materials & Methods: The library consists of an OpenCL accelerated solver for Pennes bioheat transfer equation. Different energy deposition methods like RF, MW, or laser and energy extraction method like cryogenic ablation have been combined with this implementation. For the simulation, the library takes material labels generated from segmentation of a planning image into account. Per voxel, the material parameters can be simulated state dependent, i.e. the material properties may vary depending on temperature, dehydration, and coagulation state. The simulation library has been integrated into the planning and assessment software SAFIR, enhancing the planning workflow with a patient-specific necrosis prediction that can be computed within a couple of seconds.

Results: Numerical simulation of 15min freeze-thaw cryoablation on a 128^3 computational with 0.5mm voxel size can be performed within 2sec on a standard PC. To simulate the energy extraction from the tissue, a constant temperature of -180°C is assumed at the needle"s active zone (see Fig. for an exemplary result).
Simulation of 10min MW or RF ablation on the same grid can be performed within 3sec using an electro-static approximation of energy deposition.

Conclusion: The simulation is fast enough to be integrated into an interactive planning workflow for optimal needle placement determination before the procedure. The availabilty of a fast simulation might allow to tackle challenges like intra-interventional generator steering or advanced needle placement optimizations in the future. The integration into a planning and processing workstation will ease validation of the simulation framework.

Figure 1

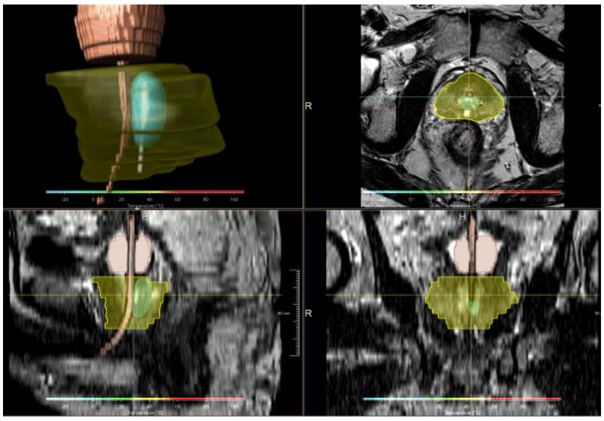

ID 27

Fast 3D-HOG (Histogram of Oriented Gradients) for Medical Imaging with GPU-Support

G. Kabelitz[1], B. Trimborn[1,2], I. Wolf[2], L. R. Schad[1]
F. Zöllner[1]
[1]University of Heidelberg, Institute for Computer Assisted Clinical Medicine, Mannheim, Germany
[2]University of Applied Sciences, Medical Informatics, Mannheim, Germany

3D images play an important role in diagnosis and image guided therapy. The HOG, introduced for the detection of pedestrians in 2D image data, was expanded by Trimborn et al. into the 3D space for medical image processing. This data contains tenfold the data from usual medical 2D images. The HOG-based similarity metric provides an alternative for MI at handling multi- and monomodal registrations. To make the HOG practicable as part of interventional image processing an efficient way to deal with the 3D data is needed.

Due to the nature of the HOG algorithm it is a candidate for a parallel implementation. The streaming processor units on the graphic card were used to achieve the acceleration together with the multicore HOG algorithm written with NVIDIAs CUDA programming language.

A pipeline process was implemented starting with a pixel-based computation of the gradient image and the spherical coordinates of those gradients. The second step attains the cell histograms for each cell. The third process computes a normalization for blocks of cell histograms which result in the HOG descriptor. All processes can be computed in parallel with synchronization steps.

The reference code is written in multi-threaded C++ code based on the Insight Toolkit. The reference and the accelerated program are run on the same computer (i5-4570 with 3.2 GHz, 16 GB RAM, GTX 1050 Ti).

The accelerated algorithm provides a HOG descriptor similar to the reference implementation in regard to the computed histogram vectors. Minor differences are

due to a different gradient computation. With this new implementation, the computational time is reduced from 250 seconds to 1.1 seconds for a single iteration of 512x512x188 medical volume.
The acceleration factor of 227 makes the HOG metric applicable for interventional use. A further time reduction can be achieved by exploiting the memory control options like memory streaming and reach for real-time registration application.

Figure 1

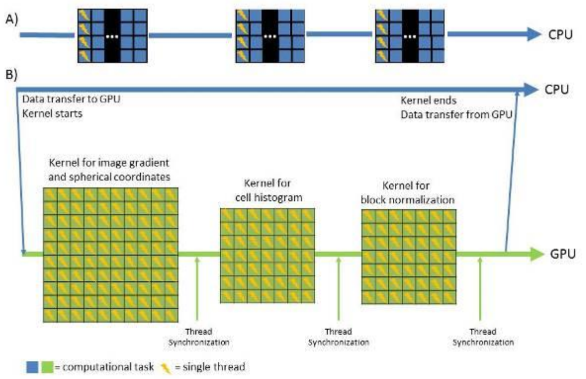

Figure: Processing pipeline on A) CPU with four parallel threads and B) GPU + CPU with up to 1024 threads parallel

ID 30

Generation of synthetic Image Data for the Evaluation of Brain Shift Compensation Methods

S. Bayer[1], A. Maier[1], M. Ostermeier[2], R. Fahrig[2]

[1]Friedrich-Alexander University, Informatik 5 Pattern Recognition Lab, Erlangen, Germany

[2]Siemens Healthcare GmbH, Forchheim, Germany

Introduction: Brain shift is the change of the position and shape of the brain during a neurosurgery procedure. This intraoperative brain deformation limits the use of preoperative image data. In order to align the pre- and intraoperative image data, sophisticated image registration methods are necessary. Thus, synthetic image data are needed for the evaluation of such methods. In this work, we introduce the generation of synthetic image data for this purpose.
Materials & methods: A binary image volume containing ventricles, vessels and soft tissue serves as input for biomechanical simulation based on finite element analysis (FEA). For the purpose of creating synthetic data, it is sufficient to simplify the soft tissue surface by computing the 2D convex hull for all axial slices. In order to ensure the quality of the meshes, the randomly distributed point cloud on the simplified surface is resampled by using Poisson Disk Sampling. Based on the resampled uniform distributed point cloud, a smoother surface model subsequently a volumetric mesh of brain with consistent mesh size is computed. Assuming linear elasticity, the deformation of the volumetric mesh is calculated with FEA considering the material properties, gravity and boundary constraints. In order to simulate the realistic C-arm CT image data, the deformed volumetric model is first transformed to a new binary image volume, and then forward projected with an image reconstruction tool.
Results: The resulting meshes and images are shown in Fig. 1. In this example, the max. simulated deformation is 10.2mm, which is in the range of clinical experience.
Conclusion: In this work we introduced a method to generate synthetic image data including soft tissue, vessels and ventricles for the evaluation of image registration methods. With the resulting images, brain shift compensation methods, especially by using 3D DSA image to update the preoperative MRI, could be evaluated.

Figure 1

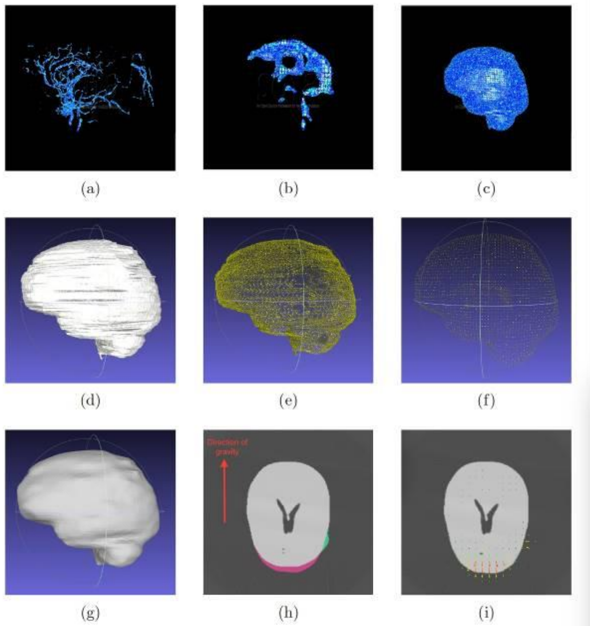

Figure 1: Above images show the volumetric mesh of the vessels (a), the ventricle (b) and the soft tissue (c). Image (d) to (g) show the soft tissue surface after computation of convex hull, the randomly distributed point cloud, the uniform distributed point cloud after using Poisson Disk Sampling and the re-generated soft tissue surface, respectively. The voxel size of the reconstructed image has the size of 1mm by 1mm by 1mm. The overlay of reconstructed image before and after deformation is shown in (h). The narrow shows the direction of the gravity. The maximum the simulated deformation of this example is 10.2mm, which is in the range of clinical experience. (i) shows the corresponding displacement field on the 142 slice in axial direction.

ID 34

Untersuchung von Artefaktverursachenden Einflüssen auf die polychromatische statistische Rekonstruktion

R. Bismark[1], O. Beuing[1], G. Rose[1]

[1]Otto-von-Guericke Universität, STIMULATE, Magdeburg, Germany

Fragestellung: CT nutzt typischerweise breite Röntgenspektren, welche zu Bildartefakten führen. Die polychromatische statistische Rekonstruktion (PSR) soll diese Artefakte reduzieren. Welchen qualitativen Einfluss auf eine PSR haben unberücksichtigte Effekte?
Methoden: Es wurde das von Elbakri et al. vorgeschlagene Verfahren einer PSR umgesetzt und auf C-Arm-CT adaptiert. Durch Metall hervorgerufene Aufhellungs-/Verdunklungsartefakte können auch

durch andere Effekte als nur durch Strahlaufhärtung hervorgerufen werden. An einem Softwarephantom wurden in den Projektionsdaten Streustrahlung und Limited-Detector-Dynamic (LDD) simuliert.

Ergebnisse: In den Abbildungen wurden jeweils gleiche Schichten der Rekonstruktionen gegenübergestellt. MSR bezeichnet im Folgenden den monochromatischen Sonderfall der PSR ohne Strahlaufhärtungskorrektur.

Abbildung 1: Simulation des Effekte Streustrahlung / LDD auf ein Softwarephantom und Vergleich mit echten CB-CT Daten eines Schweinekopfes mit Stahlnadel und klinischen Kopfblutungsdaten

Schlussfolgerungen: Streuung sorgt allgemein für Verdunklung um das Metallobjekt. Rauschen kann durch das Rekonstruktionsverfahren unterdrückt werden. Mangelnde Detektordynamik sorgt längst des Metallobjekts für Aufhellung und perpendikulär für Verdunklung. Sowohl Streuung als auch Detektordynamik "verwaschen" die klare Kante des Metallobjektes. Die PSR ist allgemein genug formuliert, um diese Effekte zu berücksichtigen zu können, was Ziel zukünftiger Arbeiten ist.

Diese Arbeit wurde vom BMBF im FC *STIMULATE* (13GW0095A) gefördert.

Referenzen

I.Elbakri and J. Fessler. Statistical image reconstruction for polyenergetic x-ray computed tomography. Medical Imaging, IEEE Transactions on ,21(2):89-99, Feb 2002.

I.A. Elbakri and J. A. Fessler. Segmentation-free statistical image reconstruction for polyenergetic x-ray computed tomography with experimental validation. Physics in Medicine and Biology, 48(15):2453, 2003.

Figure 1

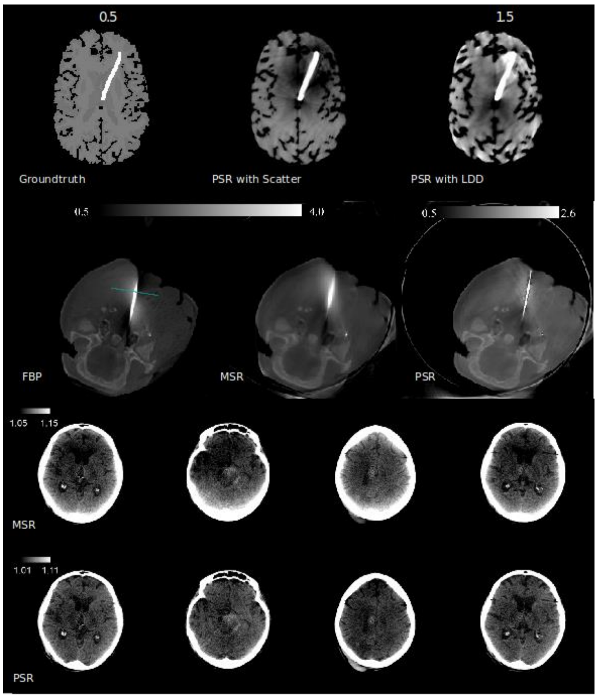

ID 44

Comparison of Deep Learning and Shape Modeling for Automatic CT-based Liver Segmentation

G. Chlebus[1], H. Meine[1], I. Endo[2], A. Schenk[1]

[1]Fraunhofer MEVIS, Bremen, Germany

[2]Yokohama City University Graduate School of Medicine, Yokohama, Japan

Introduction: The liver's varying appearance in CT images makes it very time consuming for manual delineation and challenging for automatic segmentation approaches. We investigated two automatic segmentation algorithms based on fully convolutional neural networks (FCN) and statistical shape models (SSM).

Materials & Methods: Data: We used 219 abdominal CT datasets. Each liver was manually delineated by a qualified medical staff using an established algorithm [1].

FCNN-Based Method: We trained a FCN based on the U-net architecture with four resolution levels using axial slices resampled to a 2mm isotropic voxel size [2].

SSM-Based Method: The SSM was built using the MDL algorithm for point correspondence establishment. The SSM-based segmentation process consists of several steps with varying scale and search modes [3].

Evaluation: We compared both methods on 40 CT volumes using the relative volume error (RVE) and the elapsed time(ET).

Results: The RVE was 3,8%±1,7% and 5,9%±6,8 % and the ET was 3±1s and 39±8s for the FCN- and SSM-based method, respectively. We had to exclude three cases from the evaluation, where the SSM-based approach failed to segment the liver.

Conclusion: Both investigated methods compute liver volumes with acceptable accuracy[4]. The FCN-based method is more robust and runs significantly faster than the SSM-based algorithm.

References

1. Schenk A. et al."Efficient semiautomatic segmentation of 3D objects in medical images." In Proc. of MICCAI.

2. Chlebus G. et al."Neural network-based automatic liver tumor segmentation with random forest-based candidate filtering." arxiv.org/abs/1706.00842.

3. Heimann T. et al."A shape-guided deformable model with evolutionary algorithm initialization for 3D soft tissue segmentation." In Proc. of IPMI.

4. Nakayama Y. et al."Automated hepatic volumetry for living related liver transplantation at multisection CT." Radiology Journal.

Figure 1

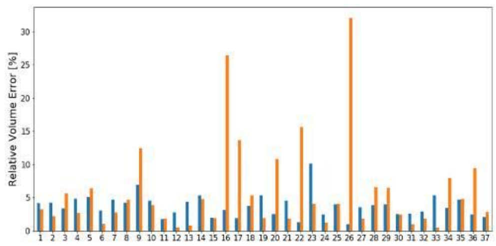

Fig.1 Relative volume difference for the FCN- (blue) and SSM-based (orange) methods.

ID 45

Application of a phenomenological beam model to cone-beam CT (CBCT) projection data for scatter correction

M. Blessing[1], M. Runz[1], F. Wenz[2]
[1]Universität Heidelberg, UMM, Experimental Radiation Oncology, Mannheim, Germany
[2]Universität Heidelberg, UMM, Radiation Oncology, Mannheim, Germany

Introduction: In radiation therapy kilovoltage cone-beam CT (kV CBCT) imaging is used for patient positioning. Due to the large size of the beam and the detector the scatter contribution for an average patient can be more than 50% of the detector signal. A phenomenological beam model was used to estimate the scatter contribution in CBCT projections. First reconstruction results are presented for a thorax phantom with integrated ball shaped tumor inlay.
Material & method: The given kV beam model was based on the dose ratio formalism: three factors characterize the measured detector signal: output factor (OF), tissue-to-air ratio (TAR) and off-axis ratio (OAR). Parameters were taken from previous measurements on an XVI CBCT system mounted to an Elekta Synergy linac. A CBCT projection data set from a thorax phantom with a ball shaped tumor inlay was acquired. It consisted of 640 projections with 1024x1024 pixels. In each projection the water-equivalent thickness was estimated based on the inverse TAR formula. The scatter contribution for each projection was calculated with Matlab based on the beam model. Reconstruction was performed based on filtered back projection. In the resulting reconstruction images the contrast c = (I_tumor − I_lung)/I_lung between tumor and lung was calculated and compared.
Results: The phenomenological beam model was tested on a complete CBCT phantom data set for the first time. The calculation time was 1.1s per projection. The contrast in the tumor area was increased from 1.35 in the original reconstruction without scatter correction to 2.96 in the corrected case. This corresponds to an improvement of 120%.
Conclusion: Application of the kV beam model to a given CBCT projection data set is a practical method to perform projection based scatter correction. The time for calculating the scatter contribution is rather long. With a C++ or a GPU implementation the calculation for a CBCT data set could be performed within a few seconds, however.

ID 49

Towards Optimal Channels for a Detection Channelized Hotelling Observer

F. Schebesch[1], A. Maier[1]
[1]Friedrich-Alexander-Universität Erlangen-Nürnberg, Pattern Recognition Lab, Erlangen, Germany

Introduction: As a method for automated image quality assessment, the channelized Hotelling observer with Laguerre-Gauss (LG) channels works well for rotationally symmetric signals on a background without preferred noise orientation. To evaluate more complex signal shapes this choice of channels might not be optimal. We extend the notion of 2D LG channels to a set of adapted channels and study the optimal shape to detect elliptical signals.
Materials & methods: A transformation of the channel functions is performed such that their level sets are rotated and scaled to become elliptical. Thereby they are parametrized by channel width, rotation angle, and a stretch factor related to ellipticity. To find a set of channels for optimal detection of the signal, the detectability index d' is used as optimization goal. We use a fixed number of nine channels (degrees 0-8). To avoid degenerate level sets for this parametrization, the goal function is constrained for all three parameters. The detectability d' is evaluated using 100 signal and 100 background images. For the background, noise correlations are induced by Gaussian filtering of normally distributed noise.
Results: Initialized with the standard circular LG pattern, the optimization process is affected by randomized data underlying the d' computation. Qualitatively, we observe that the channel width parameter converges in an expected range (about the size of the signal). The optimization results w.r.t scale and rotation parameter indicates optimal channels where the larger semi-axis of the signal ellipse is either parallel or orthogonal to the respective elliptical shapes of the channels' level sets.
Conclusion: Though the d' index yields a non-convex function w.r.t. to the given parameters, it indicates that LG channels are suboptimal for elliptical signals. A better choice is given by transformed LG functions adapted to the signal shape.
References:

1. Gallas & Barrett JOSA A 2003
2. He & Park Theranostics 2013

Figure 1

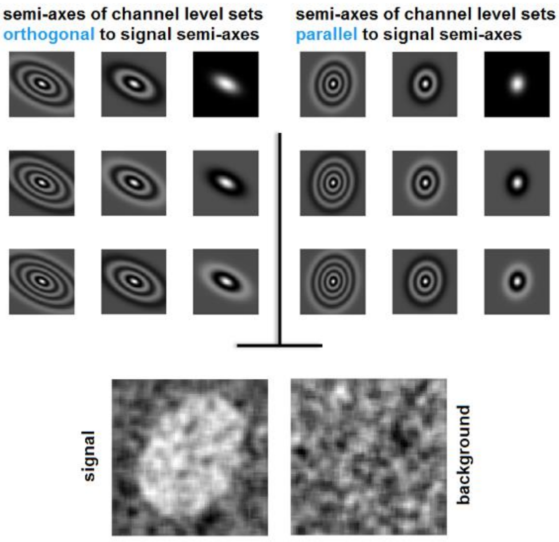

Figure: Optimizer output shows major semi-axis either orthogonal (top left) or parallel (top right) to the lesion's major semi-axis (bottom).

New approaches for interventional MRI

ID 01

Rethinking interventional MRI - is Ultrasound guidance the solution?

M. Friebe[1], R. Odenbach[1], S. Balakrishnan[1], P. Poudel[1] H. Fritzsche[1], M. Matooq[1], A. Illanes[1], J. Sanchez[1] J. Krug[1], A. Boese[1]
[1]OVGU, IMT/INKA, Magdeburg, Germany

No need to discuss the potential advantages of magnetic resonance imaging as an intraoperative diagnosis and therapy system especially for neuro applications and oncological therapies. Difficult patient access in conventional horizontal field superconductive magnets, very high investment and operational expenses, and the need for special non-ferromagnetic therapy tools have however prevented a widespread use of MRI for therapy purposes. The interventional use of MRI systems follows for the last 20+ years the strategy to use conventional diagnostic systems and add more or less complicated and expensive components (1). MRI compatible robotic systems were for example proposed to solve the patient access issue in combination with specially shielded in-room monitors and dedicated nitinol or plastic devices with no or little susceptibility related imaging artefacts (2). We are proposing to rethink that approach using an in-room portable ultrasound system that can be operated till 1m away from the opening of a 3T imaging system. The live ultrasound images are tracked using an optical inside out approach adding a camera to the ultrasound probe in combination with an optical reference marker and are immediately fused with the MRI images (3). This allows a comfortable US guided intervention and excellent patient access directly on the MRI patient bed. We combined this with a newly developed entirely mechanical MRI compatible 7DOF holding arm concept creating a very cost-efficient and effective environment that combines the advantages of MRI and US by largely avoiding the drawbacks.

(1) D. Grönemeyer, et al. Future of advanced guidance techniques by interventional CT and MRI. MITAT 10/1995; DOI:10.3109/13645709509152803
(2) G. Krombach, et al. Interventionelle MRT bei 3 Tesla. RöFo 01/2008; DOI:10.1055/s-2008-1073817
(3) S. Balakrishnan, M. Friebe, M. Real-time MRI/US fusion using inside-out tracking of virtually generated markers (ORtoMVM). CARS, Barcelona, June 2017

Figure 1

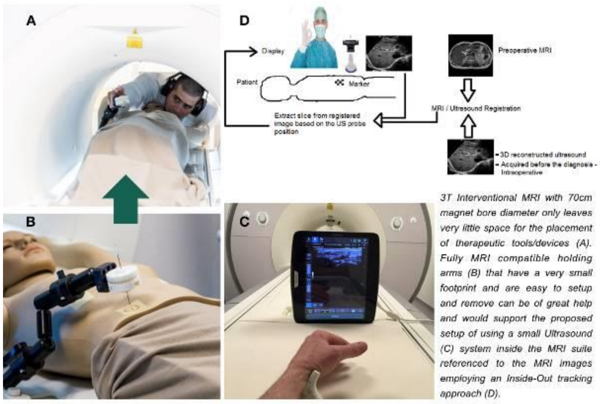

ID 03

2-D Interactive Scar Layer Visualization

T. Kurzendorfer[1,2], S. Reiml[1,2,3], A. Brost[1], D. Toth[4,5] M. Panayiotou[4], P. Mountney[6], S. Steidl[2], A. Maier[2]
[1]Siemens Healthcare GmbH, Forchheim, Germany
[2]Friedrich-Alexander University Erlangen-Nuremberg, Pattern Recognition Lab , Erlangen, Germany
[3]Friedrich-Alexander University Erlangen-Nuremberg, Erlangen, Germany
[4]King's College London, 3Department of Biomedical Engineering, London, United Kingdom
[5]Siemens Healthcare Ltd, Frimley, United Kingdom
[6]Siemens Healthcare GmbH, Medical Imaging Technologies, Princeton, United States

Introduction: Cardiac magnetic resonance imaging (MRI) is used in clinical routine for diagnosis, as it can provide information on morphology, perfusion, or tissue viability. For patients suffering from heart failure the viability analysis of the myocardium is critical. However, the transmurality of the scar can be challenging to interpret, but is of high value for therapy planning.

The location and transmurality of the scar is often examined by looking at the slices of the LGE-MRI. Another method is the visualization within an AHA bull"s eye plot (BEP), where the scar transmurality is presented in percentage [1], see Fig. A. Or the scar mesh can be projected on the BEP, as depicted in Fig. B. However, with these methods it is not possible to differentiate between endocardial and epicardial scar. Therefore, we propose a new 2-D interactive scar layer visualization using the BEP.

Materials & Methods: The prior segmentation of the myocardial scar is required [2]. Afterwards, the segmentation mask is divided into three layers, resulting in an endocardial, mid-cavity and epicardial layer [3]. These layers can then be projected on the BEP, see Fig. D-F, or overlaid on top of each other, as illustrated in Fig. C. If all layers add up, the scar is transmural.

Results: The myocardial scar tissue can be observed from the endocardium to the epicardium and ideal points for lead placement for cardiac resynchronization therapy can be found easier compared to traditional decision making in 2-D.

Conclusion: A novel method for interactive 2-D visualization of the scar layers within an AHA BEP has been presented. This visualization method can give precise information about the location and transmurality of the myocardial scarring.

Disclaimer: The methods and information presented in this paper are based on research and are not commercially available.

References:

[1] Reiml et al. SPIE 2016

[2] Suinesiaputra et al. MedIA 2014

[3] Reiml et al. BVM 2017

Figure 1

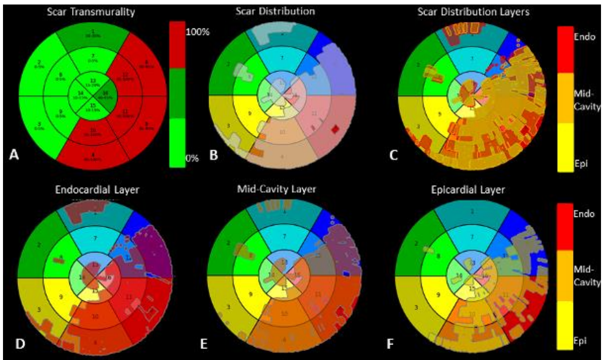

Figure: (A) Bull's eye plot (BEP) of the left ventricle showing the scar transmurality as percentage and color coding. (B) Shows the BEP with the scar volume. (C) Depicts the BEP with three scar layers, where the red layer corresponds to endocardial scar, the orange to mid-cavity and the yellow to epicardial scar. (D) Endocardial scar distribution. (E) Mid-cardial scar distribution. (F) Epicardial scar distribution.

ID 12

Fan-beam Projection Image Acquisition using MRI

C. Syben[1], B. Stimpel[1], M. Leghissa[2], A. Dörfler[3]
A. Maier[1]

[1]Friedrich-Alexander-Universität Erlangen-Nürnberg (FAU), Department of Computer Science 5 , Erlangen, Germany
[2]Siemens Healthcare GmbH, Forchheim, Germany
[3]Universitätsklinikum Erlangen, Kopfkliniken – Neuroradiologie, Erlangen, Germany

Introduction: Real-time image acquisition is crucial for interventional MRI. The acquisition of parallel projection images is fast but lacks perspective distortion similar to X-ray fluoroscopy. We introduce a k-space sampling to create projection images with perspective distortion and evaluate the density of the necessary k-space sampling to achieve suitable results.

Materials & Methods: The Fourier-slice-theorem can be used to identify the part of the k-space where a fan-beam projection is contributing to. The lines perpendicular to the outer rays define the border of the wedge in Fourier space, where the information of fan-beam projection is placed. Sampling the lines perpendicular to each ray and applying the inverse Fourier transform gives a stack of parallel projections, which can be resampled to a fan-beam projection by

$\Theta=\gamma+\beta$

$s=d_{si}+\sin\gamma$,

where γ is the half fan-angle, β the angle between the central ray and the coordinate axis and d_{si} is the source to isocenter distance. Θ describes the rotation angle of a detector acquiring parallel beam and is the respective pixel. The projections are generated from a slice of a head phantom. A ray-driven forward projection is used as ground truth (GT). A detector with 511 pixels is assumed i.e. 511 lines in k-space correspond to full sampling. In this case, highly redundant data is acquired. Thus, undersampling factors with equiangular spacing, including the central and the two outer rays, are investigated.

Results: Fig. 1 shows that the resampling error is nearly constant down to 15 projections. Using less projections increases the error up to 5% in maximum for the 3 projection case (see Fig. 1.D).

Conclusion: The results show that we can create fan-beam projections with a perspective distortion while the amount of sampling lines in the k-space is minimal. Adapting the minimal k-space sampling to cone-beam enables for fast acquisition of projection images with the same perspective distortion as angiography systems.

Figure 1

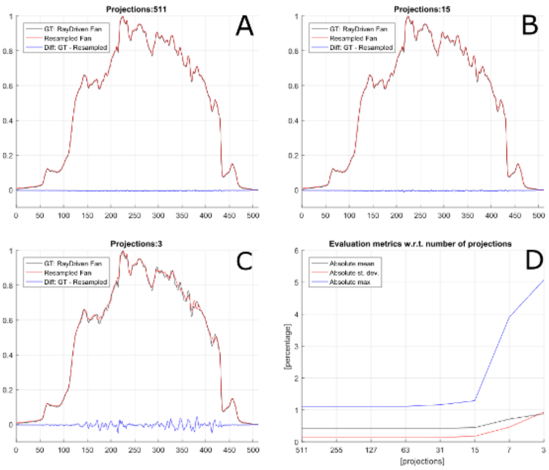

ID 15

Proof of Concept of a Hybrid MRI-Ablation System

T. Gerlach[1], E. Pannicke[1], U. Kägebein[1], O. Speck[1]
R. Vick[1]
[1]Otto-von-Guericke University, Magdeburg, Germany

Introduction: Due to its superior soft tissue contrast and possibility of temperature acquisition, MRI represents a promising tool for guiding ablation procedures. Fig. 1 shows a set-up for an MRI-guided RFA-procedure [1]. The RF generator is not MR compatible and has to be placed outside the MR room. Interferences created by the electronic device itself must be attenuated by filters [2]. Otherwise intra-operative imaging is not possible. We therefore propose a hybrid MRI ablation system, where the ablation electrode is connected to the RF amplifier of the MRI (seen fig. 2). The RF ablation power is directly generated by the used imaging sequence. The following abstract will present first results of this system.

Materials and Methods: Validations were done on a 3T MRI system using a turbo spin echo sequence (see fig.3). A bipolar electrode was made from a semi-rigid coaxial cable. The electrode was placed in a polyacrylamide phantom. Sensors measured the temperatures during the ablation.

Result: Figure 4 shows the temperature development during the ablation procedure. The sensor 1 measured a strong temperature increase once the sequence started. Sensor 2 and 3 revealed a slow increase whereas no change was detected by sensor 4.

Conclusion: It has been shown that the proposed hybrid MRI ablation system can generate temperatures which could lead to irreversible tissue damage. Carbonization next to the electrode showed that even temperatures above 100°C were generated. Further improvements of this system shall involve MR thermometry.

References:

[1] Jolesz. "Intraoperative Imaging and Image-Guided Therapy", Springer 2014

[2] Will. "MR-Compatible RF Ablation System for Online Treatment Monitoring Using MR Thermometry", IEEE Engineering in Medicine and Biology Society 2010

Acknowledgment: This work was funded by the German Federal Ministry of Education and Research (BMBF) within the research campus STIMULATE (13GW0095A).

Figure 1

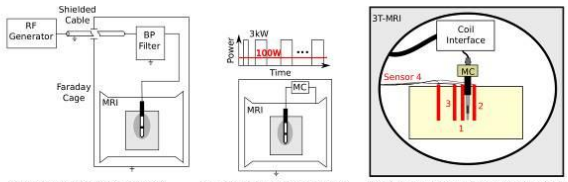

Figure 1: Set-up for MRI-Guided RFA

Figure 2: Set-up for hybrid MRI ablation system

Figure 3: Test arrangement for Hybrid system

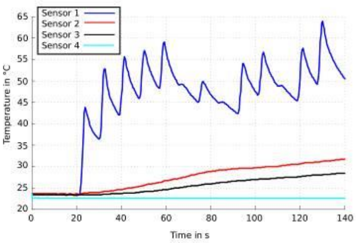

Figure 4: Temperature development during a 3D-TSE sequence

Figure 5: Carbonation formed during the procedure

ID 32

Intuitive instrument navigation for MR guided percutaneous procedures

U. Kägebein[1], E. Pannicke[2], F. K. Wacker[3], O. Speck[1]
B. Hensen[3]
[1]Otto-von-Guericke University Magdeburg, Biomedical Magnetic Resonance, Magdeburg, Germany
[2]Otto-von-Guericke University Magdeburg, Electromagnetic Compatibility, Magdeburg, Germany
[3]Hannover Medical School, Hannover, Germany

Question: MRI as guidance tool for minimal invasive procedures is characterized by an excellent soft-tissue contrast and lack of ionizing radiation. Up to date one of the main drawbacks of MRI-guided procedures is its complex often time-consuming workflow [1]. The development of an appropriate guidance support is essential to simplify and shorten the intervention. We present a new imaging and tracking sequence enabling intuitive instrument navigation with the aid of an optical Moiré Phase (MP) tracking system inside the MRI magnet.

Method: For real time needle guidance four MP markers were rigidly attached to a ceramic needle (see Fig. 1a). A gradient echo sequence was modified to align two perpendicular imaging planes along the calibrated ceramic needle centered at the needle tip. The imaging planes are updated according to the motion of the MP markers being tracked by a newly developed camera system. The images and additional guiding information were displayed in a mosaic manner. The system was evaluated by one medical doctor targeting five rubber O-rings (Øinner=10mm) embedded in a custom-made phantom. The mean targeting time was recorded and the mean target deviation was measured from 3D acquisitions after the procedure.

Result: Based on the constant feedback of the needle trajectory, its extension and the target tip distance, the user could easily correct deviation from the target trajectory on the fly (see Fig.1b). A short targeting time of t=76.2 s ± 2.5 s and a low mean target error of 1,1 mm ± 0,3 mm could be reached.

Conclusion: Compared to other publications the mean targeting time and deviation with the system used are promising[1, 2]. In order to confirm this pilot study, the next step shall include more users and puncture experiments for a detailed evaluation of the guidance system.

References:

[1] 10.1002/jmri.23894.

[2] 10.1371/journal.pone.0134370.

Acknowledgment: The work of this paper is funded by the BMBF under grant number '13GW0095A' and '13GW0095C'

Figure 1

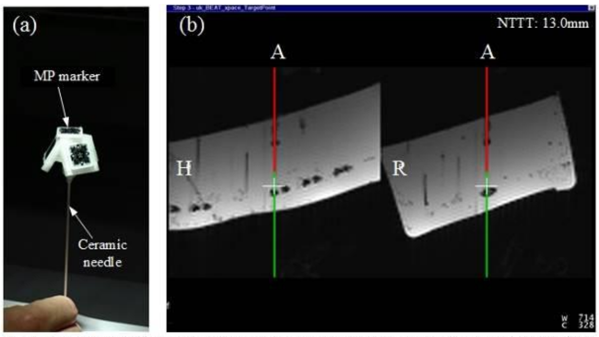

Fig. 1 *Intuitive instrument navigation. a| Ceramic needle with attached MP markers using an appropriate holding device. b| Images of the real time needle guidance displayed in a mosaic manner with additional information about the needle trajectory (red line), its extension (green line), target tip distance (white cross), needle tip to target distance (NTTT) and slice orientation (H=head, A=anterior, R = right).*

ID 33

Noise Reduction in Magnetic Resonance Images for Thermometry by Synchronisation of a Microwave Ablation System

M. Prier[1], E. Pannicke[2], U. Kägebein[1], G. Rose[3]
O. Speck[1], T. Ormsby[4], B. Hensen[5]

[1]Otto-von-Guericke University, Biomedical Magnetic Resonance, Magdeburg, Germany

[2]Otto-von-Guericke University, Electromagnetic Compatibility, Magdeburg, Germany

[3]Otto-von-Guericke University, Healthcare Telematics and Medical Engineering, Magdeburg, Germany

[4]MedWaves, Inc., San Diego, United States

[5]Medizinische Hochschule Hannover, Hannover, Germany

Question: MRI for guiding and monitoring interventional procedures like thermal ablations is attractive due to a high soft tissue contrast and the ability to measure the applied heat by thermometry. Microwave ablation (MWA) achieve ablation volumes of up to 5cm in diameter and is more resistant to heat sink effects and changes of the tissue impedance than RF ablation systems [1]. Due to their working frequency of about 915MHz and MRI artefact free antenna-probes MWA could be utilized for MR-guided tumour ablation. This provides the opportunity to monitor the development of the necrosis zone in real-time by measuring the temperature changes. However, state of the art MWA system show image artefacts and a signal-to-noise-ratio (SNR) increase. The following abstract will present a first approach to improve the image quality during simultaneous MWA and MRI.

Methods: The electrical noise is induced by the continuous running MWA generator. By synchronizing the ablation procedure and the image acquisition via the the breathing cycle of the patient (Fig.1) it was possible to pause the MWA temporarily, thus reducing the noise contribution. The intern power controlling of the generator will compensate the ablation time loss.

Results: The SNR dependant standard deviation of the temperature ΔT is a measure for the accuracy of the estimated necrosis zone. In a phantom measurement an ablation is executed and images are acquired. The reference images without the ablation system have a mean SNR = 61 and ΔT = 0.86K. The continuous ablation reduces the SNR = 11 and ΔT = 1.48K(+72%) (Fig.2). With the synchronized generator the SNR is lifted back to 32 and ΔT = 1.22K(+42%) (Fig.3).

Conclusions: The synchronization of the MWA generator triples the MR image quality thus creating a basis for reliable thermometry while MWA ablation.

References:

[1] M. G. Lubner, Microwave tumor ablation: mechanism of action, clinical results and devices, J. V. I. Rad. 21 192-203, 2010

Figure 1

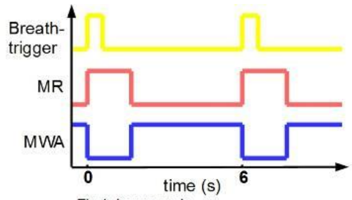

Fig.1: Image cycle

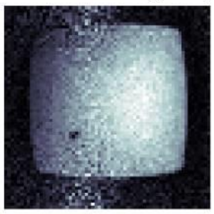

Fig.2: Continious Ablation

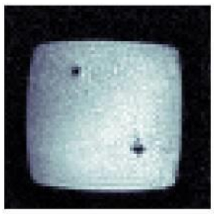

Fig.3: Synchronized Ablation

ID 37

Optimized workflow for interventional magnetic resonance guided microwave ablation in the liver

B. Hensen[1], U. Kägebein[2], O. Speck[2], E. Pannicke[3]
F. K. Wacker[1]

[1]Hannover Medical School, Hannover, Germany
[2]Otto-von-Guericke University Magdeburg, Biomedical Magnetic Resonance, Magdeburg, Germany
[3]Otto-von-Guericke University Magdeburg, Electromagnetic Compatibility, Magdeburg, Germany

Introduction: Compared to CT or ultrasound MRI has superior soft tissue contrast, lacks ionizing radiation and provides morphologic as well functional information. Interventional MRI (iMRI) is still somewhat limited to specialized clinical centers due to access and workflow limitations (1,2). In order to make iMRI more time efficient, workflow and interventional tools are essential. Our goal was, to provide setup and techniques that will help to facilitate MRI guided thermal ablation in a standard short and wide bore MR magnet.

Material and Methods: With the patient in general anesthesia, baseline imaging is performed to visualize target lesions. For access, entry and target points are defined. The fingertipping method was used to define and mark the skin entry point. After skin prepping and sterile covering, a 4 channel flex coil was positioned. After local anesthesia was used, the insertion of the microwave antenna (Medwaves AveCure) was performed under real-time MRI imaging guidance with the aid of the interactive real-time TrueFISP sequence. After reaching the final destination, the lesion was ablated for 10 min while conventional thermometry images were acquired. After the ablation, the antenna was pulled back and a 3D postcontrast dataset was acquired to determine the necrosis zone. Procedure time was recorded.

Results: Preparation time ranges from 30 to 42 minutes. Interactive imaging control facilitated swift positioning of the antenna into the desired location (see Fig. 1). Once the needle was inserted, targeting ranged from 85 to 621 seconds. Thermometry images acquired during the ablation revealed an hot spot increasing in size and temperature during energy application. The post-contrast control scans visualize coverage of the lesion and correlate well with thermometry.

Conclusion: Using a well-planned workflow, MR guided interventions on a wide closed bore MR magnet are clinically feasible.

References:

[1] 10.1002/jmri.21269 [2] 10.1148/radiol.12120117

Figure 1

Figure 1. *BEAT_IRTTT sequence with TRUFI contrast shows the applicator in the target region in the liver dome.*
(Acknowledgment: The work of this paper is partly funded by the Federal Ministry of Education and Research within the Forschungscampus STIMULATE under grant number '13GW0095C' and '13GW0095A'.)

ID 38

Towards Touchless Control of MR Scanners during MR-guided Interventions

B. Hatscher[1], C. Hansen[1], E. Pannicke[1], U. Kägebein[1]
F. Wacker[2], B. Hensen[2]

[1]Otto-von-Guericke Universität Magdeburg, Magdeburg, Germany
[2]Medizinische Hochschule Hannover, Hannover, Germany

Introduction: Interacting with the MRI during MR-guided interventions is a cumbersome task. Physicians have to use MR-save control panels, which are often not available or unintuitive. Alternatively, interaction tasks are delegated to an assistant at the control panel verbally, which requires extra equipment due to noise and depends on the assistant"s level of experience. Therefore, we propose to control a MR scanner via touchless gestures.

Materials & methods: In an intraoperative scenario, only certain commands are required to support the workflow of the physician. In cooperation with domain experts, we identified the need for the following functions to be accessible during interventions:

- Sequence control
  - Sequence selection
  - Sequence activation/deactivation
  - Set sequence quality/time
  - Windowing
- Image plane adjustment
  - Set plane orientation (parallel/perpendicular)
  - Translate/Rotate image plane

Considering the conditions in an MRI setup, camera based gesture sensing seems to be a promising approach. When it comes to positioning, gestures need to be detected during complicated settings such as needle interventions which require the physician to lean into the bore. Therefore, a small, MR-save gesture detection device is required.

Conclusion: As next steps, we plan to verify the intraoperatively required functions by analyzing workflows of MR-guided interventions and consult domain experts. The results will serve as foundation for our touchless control application. For the human-computer interface, a set of adequate gestures has to be found, implemented and tested under intraoperative conditions.

In the long run, we believe control of MRI sequences and image planes using a in-room MRI safe device (e.g. gesture-supported MR-interventions) will save time, reduce communication errors and result in a saver, less stressful experience for the patient as well as the physician.

Federal Ministry of Education and Research (BMBF) grant number: 13GW0095A

ID 41

High-Speed-Communication into the MRI-Bore

M. Knoll[1], S. Orsolini[2], E. Pannicke[1], S. Diciotti[2], R. Vick[1]
[1]Otto-von-Guericke Universität Magdeburg, Department Electromagnetic Compatibility, Magdeburg, Germany
[2]Universita di Bologna, Dipartimento di Ingegneria dell'Energia Elettrica e dell'Informazione, Bologna, Italy

Introduction: In developing new measuring and actuating equipment for the MRI, we and other scientists frequently reimplement communication-interfaces. Because of challenges involved with sending data in and out of a highly interfering environment, this often inhibits fast prototyping and degrades measuring performance because of bandwidth limitations. We are proposing a standardized, yet flexible interface, simplifying the development of equipment communicating right into the MRI bore.

Material & Methods: Out of various communication methods we narrowed down to evaluating two, wireless IEEE 802.11 and 100BASE-FX fibre optic. Our custom electronics are battery powered and inherently isolated. Inside the bore a ARM Cortex-M4F DSP provides communication interfaces and, if the user desires, capacity for preprocessing data. We also provide software for interfacing these devices and implementing application-specific software.

Results: Our evaluation of the prototypes in our MRI showed advantages and limitations of both wireless and fibre interfaces. We were able to use prototype hardware for measuring gradients inside the MRI and used that data to improve other hardware projects. The methods we developed for shielding and protecting electronics could also be applied in other high-EMI environments.

Conclusion: The feasibility of both concepts could be proven and we are continuing testing and development. We also desire to improve usability and performance of our prototypes and are pursuing further uses for this technology. In our own projects these interfaces already proved useful and we hope to provide an easy-to-use tool for other researchers soon.

ID 42

Rapid test setup to evaluate interventional mri coils designs.

E. Pannicke[1], R. Vick[1]
[1]Otto-von-Guericke University, Institute of Medical Engineering, Magdeburg, Germany

Question: A new method to evaluate mri coil designs is introduced, which aims to simplify its prototyp development. In contrast to the well establised measurement of port quantities or signal-to-noise estimation from MR-images, this method is suited to directly obtain the normalized field distribution of a coil and can therefore deliver a scanner independent standard.

Theory: To estimate the magnetic field H_a of an arbitrary coil a the principle of reciprocity is used [1]:

$U_b*I_b= \int j*H*\omega*M_b\,dv$

, where U_b is the voltage induced in the coil by the magnetic dipole M_b and I_a is the electrical current generating the field H_a of the coil at the same position of M_b. Replacing M_b*dv by a small probe the normalized fields can be acquired by measuring the scattering parameters

$H_a/I_a = S_{ab}/(1-S_{bb})*2*Zo/j/A_p$

,where S_{ab} is the transmission from probe b to mri coil a, Z_0 the characteristic impedance and A_p a geometrical scaling factor.

Method & Results: During the measurement a probe is moved through the volume to estimate the field distribution in the volume. The probe consists of orthogonally alligned loops. A DE-Optimization algorithm was implemented to calibrate the probe properly [2]. To optimize the number and position of sampling points in space a FEM-based algorithm was developed to ensure an optimal distance between all samples by preserving all necessary information of the distribution. Algorithms to reconstruct the field distribution from "uncomplete" measurements were also tested and could reduce the overall duration by 50-60%. Reference simulations of a well defined mri "standard" coil were conducted and compared to measurements to show the feasibility of the method (Fig.1).

Conclusion: The results for the standard coil and an actual MRI receive coil demonstrate that this method could be used to analyze the field distribution of MRI-coils outside the scanner.

References:

[1] Rumsey,PhysRev(1954):1483
[2] Wu,JourMathPhy(1962):1301-1304

Figure 1

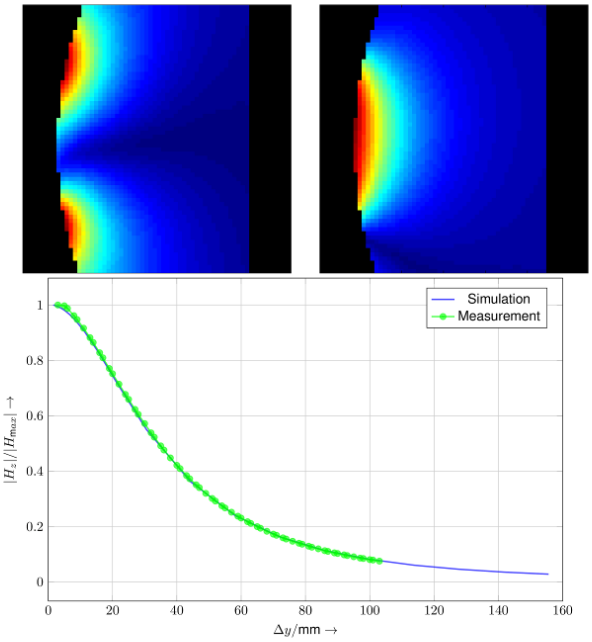

ID 50

Offcenter imaging during magnetic resonance interventions to improve patient access.

E. Pannicke[1], F. Lüsebrink[2], U. Kägebein[2], B. Hensen[3]
F. Wacker[3], O. Speck[2], R. Vick[1]

[1]Otto-von-Guericke University, Institute of Medical Engineering, Magdeburg, Germany
[2]Otto-von.Guericke University, Biomedical Magnetic Resonance, Magdeburg, Germany
[3]Hannover Medical School, Diagnostiv and Interventional Radiology, Hannover, Germany

Question: Patient access is one of the pressing issues in introducing interventional magnetic resonance imaging to the clinical routine. Because of the bore's length the In-Out-Method is mostly prefered at scanners with small diameters. However, the authors think that the freehand method should be prefered for such interventional procedures[1]. The question arising from this dilemma is – Can we bring the patient out of the isocenter to improve access for the interventionalist?

Methods: In this study we conducted experiments to see how far away from the isocenter a patient could be imaged. Outside the regular field of view of a scanner its gradient is nonlinear and the B0 field is not homogenous.

The subject under test was a phantom filled with saline solution (Siemens, Germany). A modified spin echo sequence, which allowed altering the receiver bandwidth, was used for imaging. The coil setup consisted of a 2-channel TX/RX-Birdcage (Rapid, Würzburg, Germany). The whole arrangement was sequently moved out of the isocenter towards the bore entry with a maximum distance of 20cm on the scanner's z-axis. To correct for geometrical distortions due to gradient's non linearity a unwrapping algorithm was used [2].

Results: Several limits were encountered during moving the object along the z-axis. Prior experiments showed that the scanners body coils are the most limiting factor in the signal acquisition change. Its effective volume of excitation is much smaller than the linear region of the gradients. A TX/RX-coil is therefore mandatory. For distances larger than 10cm strong geometric artifacts were observed in the images. The applied correction was able to reduce these artifacts up to 15cm away from the isocenter. However, signal intensity variations were still visible, since the applied method does only correct geometric distortions.

[1] Fischbach,F;CardiovascInterventRadiol;2011;34(11):188-92
[2] Janke,A;MagnResonMed;2004;52(1):115-22

Figure 1

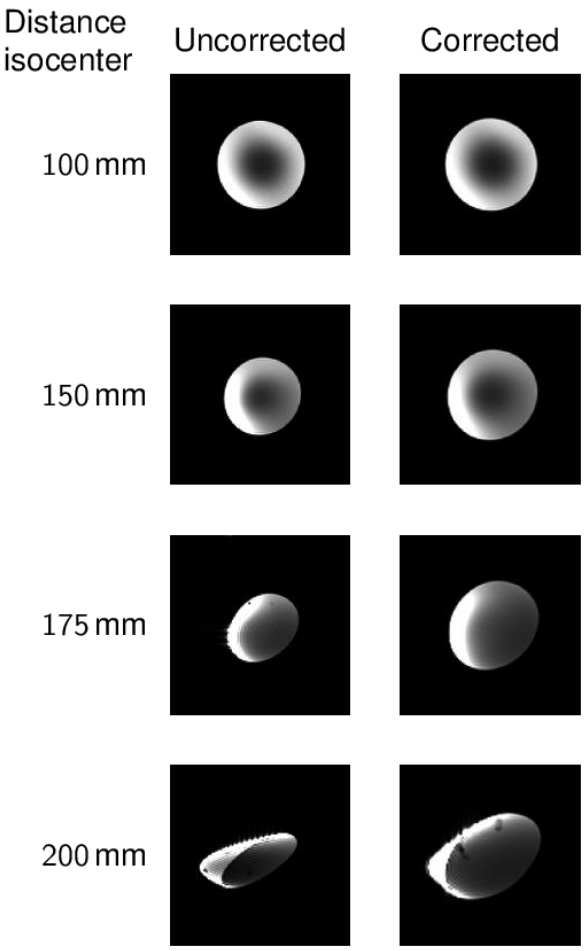

ID 51

Interventional coil design

E. Pannicke[1], R. Vick[1]

[1]Otto-von-Guericke University, Institute of Medical Engineering, Magdeburg, Germany

Question: Commercial available coils are not optimal for interventional procedures due to their limited handling. Aim of this study was to show the feasibility of a minimal coil design to improve its handling during interventional procedures.

Methods: Aim of this study was to reduce the overall components on one loop to be able to integrate it into a drape. Lumped components on a MRI loop coil are required for tuning and matching and passive decoupling. First aspect was accomplished by a self resonance design consisting of overlapping conductor tracks. Numerical studies showed that such systems can be easily tuned by the ratio of overlapping and non-overlapping tracks. As highly resonant system passive decoupling becomes crucial for a proper performance. A λ/4-transformation circuit in combination with PIN-Diodes were utilized to achieve the so called preamplifier decoupling for the transmit and receive case. This technique suppress the currents in the loop and therefore minimizes its interaction with external fields.

Validation experiments were conducted on a 3T scanner (Skyra, Erlangen, Germany) on a human like phantom.

Results: The results of the mri measurement are shown in Fig.1.

Conclusion: The proposed design can serve as interventional drape coil. This is accomplished by reducing the number of lumped components necessary.

Figure 1

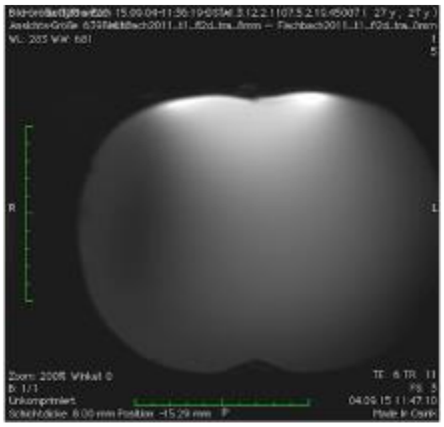

New tools and methods for image guided interventions

ID 02

Feasibility of multi-frequency wave actuation for magnetic resonance elastography of a novel actuator using centrifugal force

W. Neumann[1], A. Bichert[1], J. Fleischhauer[1], L. R. Schad[1] F. G. Zöllner[1]

[1]Universität Heidelberg, Medizinische Fakultät Mannheim, Lehrstuhl für Computerunterstützte Klinische Medizin, Mannheim, Germany

Image-guided interventions rely on previous acquired CT and MRI images, e.g. for accurate needle path planning during automated biopsies. Data sets of magnetic resonance elastography (MRE) acquired during a diagnostic MRI examination can quantify and map tissue elasticities of penetrated soft tissues and organs, which is a valuable a priori information for the pre-operative planning phase.

We developed a novel 3D-printed pneumatically driven actuator for MRE. It generates shear waves based on the principle of centrifugal force. This work presents the evaluation of technical parameters of the pneumatic turbine as well as a feasibility study of multi-frequency actuation on an anthropomorphic phantom.

The actuator is capable of generating mechanical sinusoidal shear waves in a range of 20 Hz to 180 Hz. The generated force increases quadratically with increasing frequencies. A silicon-based based phantom with a spherical inclusion 2.3 times stiffer than the background was used for MRE with actuation frequencies of 80 Hz and 100 Hz. Images were acquired in a 1.5 T whole-body scanner with an EPI-based sequence. No artefacts were induced by the actuator and the phantom was penetrated entirely with shear waves. The phase length is longer in the stiffer inclusion compared to the softer background material (**Fig. 1**) which is in accordance to the expected results.

In conclusion, this work present a simple set up of an actuator using centrifugal force for MRE. It can be incorporated within existing equipment in the clinics. It is MR safe and does not induce image artefacts. Its design is adaptable and reproducible through 3D-printing. The actuator generates sufficiently large wave amplitudes to entirely penetrate the phantom and the transducer amplitude is preserved at higher actuation frequencies.

The acquired MRE elasticity maps can thus be included in future simulations of more accurate and personalized needle path planning for image guided interventions.

Figure 1

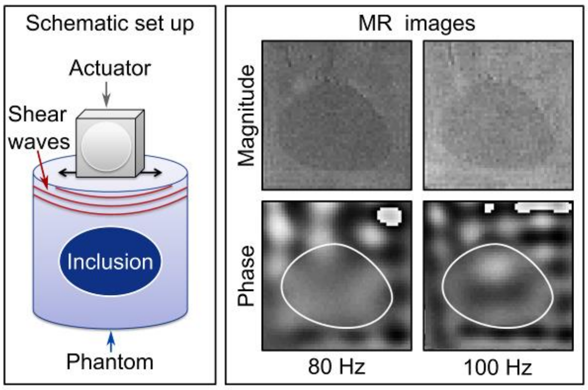

ID 13

SAFE: Software Support and Assistance Systems for Minimally Invasive Neurovascular Interventions

T. Pätz[1], L. Karstensen[2]

[1]Fraunhofer MEVIS, Bremen, Germany

[2]Fraunhofer IPA, Projektgruppe für die Automatisierung in der Medizin und Biotechnologie PAMB, Mannheim, Germany

Introduction: We present a project aiming to develop a highly-integrated planning and assistant system for minimal-invasive neurovascular interventions. The system consists of hardware and software components to especially ease and shorten the time-consuming and difficult navigation part of such interventions.

Methods: The envisioned system will contain a software component for virtual therapy planning based on the vascular system segmented on diagnostic image data. The targets selected in the planning step will be transferred to an intra-interventional software component featuring registration/fusion of intra-interventional fluoroscopic images and the planning data and catheter tracking in the fluoroscopic images based on fiber-optical shape sensing technology. Catheter control will be possible using a robotic catheter control that calculates optimal catheter trajectories by means of a catheter simulation. Furthermore, the catheter control will provide audio and/or haptic feedback to provide navigation aids to the physician without interferring with the manual catheter control workflow. Further components will target towards flow simulation in the virtual planning step and intra-interventional flow measurements by means of fiber-optical anemometry.

Results: The project is in the specification and proof-of-concept phase of the individual components. There have been promising initial results for the key components fiber-optical catheter tracking, real-time registration of fluoroscopic and diagnostic 3D images, and the fiber-optical anemometry. However, system integration and systematic validation of the components has not been started yet.

Conclusion: The individual components and the integrated system might provide innovative solutions for the growing and highly-specialized area of endovascular neuro interventions. This might enable more phycians to perform such procedures and help patients to retrieve personalized and optimized interventions on time.

Figure 1

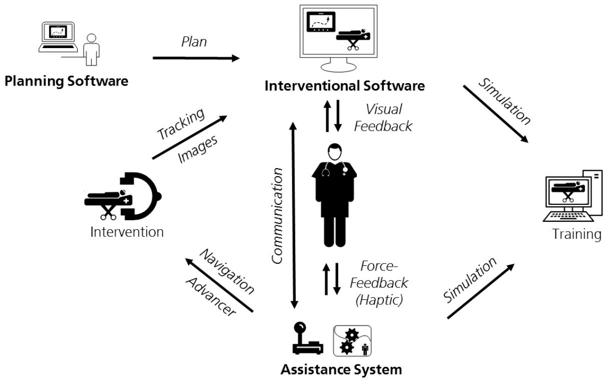

ID 16

Arbitrary cone beam scan trajectory calibration for X-ray imaging

K. Chung[1], G. Kabelitz[1], L. Schad[1], F. Zöllner[1]

[1]Heidelberg University, Computer Assisted Clinical Medicine, Mannheim, Germany

Question: Minimal invasive surgeries heavily rely on imaging modalities such as X-ray imaging. In order to reduce dose exposure whilst preserving a good image quality, research groups have started researching task-based scan protocols. With arbitrary scan trajectories, e.g. the detectability of critical objects can be enhanced. Because the exact geometry of the imaging system is required for a sufficient image reconstruction, the scan trajectories must be calibrated. We present a calibration algorithm for arbitrary scan trajectories with a custom-build calibration phantom. To evaluate the algorithm, a circular tomosynthesis scan trajectory (a) was calibrated.

Methods: The projection of a point in a 3D volume onto the detector plane can be expressed by matrix multiplications (projection matrix formalism). To describe the cone beam imaging geometry, the following nine parameters were used:

- Position of the source in x/y/z-coordinates
- Position of the detector center in x/y/z-coordinates
- Tilting/rotation angles of the detector plane

Every distortion/misalignment of any of these parameters causes a specific projection error on the detector plane as exemplary depicted (b). These errors can be quantified and stored in a matrix for every point of the scanned volume. Using the error matrix, imaging geometry flaws can be iteratively corrected.

Results: A circular tomosynthesis scan trajectory (a) was implemented on an interventional C-arm cone beam X-ray system (ARTIS zeego, Siemens Healthineers, Forchheim). The calibration routine corrected the imaging geometry successfully. The reconstruction with the calibrated data shows less geometric distortions and artefacts (c).

Conclusion: The presented calibration algorithm is capable of calibrating arbitrary scan trajectories. The reconstruction benefits from the corrected imaging geometries. In the future, we want to optimize the algorithm and test it on more complex scan trajectories.

Figure 1

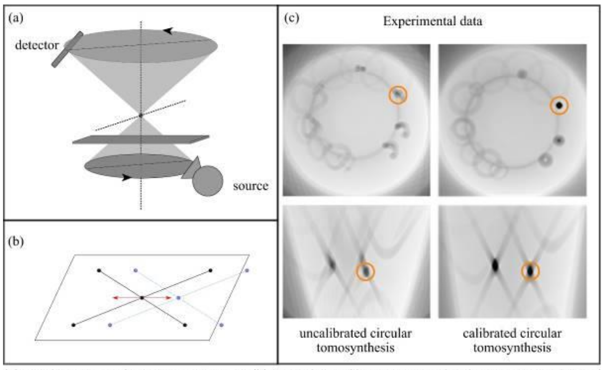

(a) circular tomosynthesis scan trajectory; (b) exemplary calibration error: the detector is translational shifted (red arrows), therefore the measured projection (blue) differs from the expected position (black); (c) comparison of the reconstruction with and without calibration

ID 17

Auditory Display for Supporting Image-Guided Medical Instrument Navigation in Tunnel-like Scenarios

D. Black[1,2,3], T. Ziemer[4], C. Rieder[2], H. Hahn[2,3]
R. Kikinis[1,2,5]

[1]University of Bremen, Medical Image Computing, Bremen, Germany
[2]Fraunhofer MEVIS, Bremen, Germany
[3]Jacobs University, Bremen, Germany
[4]University of Bremen, Cognitive Systems Group, Bremen, Germany
[5]Brigham and Women's Hospital, Surgical Planning Laboratory, Boston, United States

Introduction: Navigation information for clinical applications using tracked instruments is typically shown on a screen in an operating room. Instruments, e.g., dissector, needle, or fraise, are viewed in relation to preoperative planning data. Although visual methods provide useful information, clinicians must remove their view from the patient to view monitors often placed in uncomfortable locations. Transmitting navigation cues using auditory display instead of a screen can benefit the clinician in numerous ways, foremost by allowing visual attention to remain on the patient while receiving useful information about the placement of a tracked tool.

Methods: This work presents two auditory display methods to supplement visual methods for placement of medical instruments in cognitively demanding tunnel-like navigation tasks, such as for needle placement, image-guided laparoscopy, or transnasal robotcs, where an instrument must be navigated to remain on the origin of a plane orthogonal to the line to a planned target. Two novel auditory displays for instrument guidance are described: first, a note-based synthesizer that employs glissando direction (pitch bending) and stereo mix, and second, a virtual choir of sung syllables that guide the clinician towards a planned path.

Results: Results of a first evaluation of users using a think-aloud usability show that both methods can provide complete screen-free guidance to guide towards a target inside a virtual 3d tunnel model of a transnasal passage. The work describes benefits and drawbacks each method, providing insight for future applications of auditory display for medical navigation.

Conclusion: The methods allow blind guidance but are intended for future use in hybrid audiovisual solutions to provide an optimal combination of in-depth visualization and quick, efficient auditory cues when the clinician needs them most, thus increasing usability of navigation aids.

ID 21

Interventional imaging system concept based on miniaturized X-ray tubes (FlexScan)

S. Lagotzki[1], M. Friebe[1], A. Boese[1]

[1]Otto-von-Guericke University Magdeburg, IMT - INKA, Magdeburg, Germany

Introduction: Conventional X-ray systems are designed to cover a broad range of use, providing many features. These multi-use-systems are a compromise in terms of functionality, usability and cost. A dedicated, intuitive and practical X-ray system could improve the workflow of some image-guided procedures significantly. Based on miniaturized X-ray tubes, we developed a concept for an X-ray system focussing on extremity interventions in small and dedicated clinic/surgery setups (FlexScan).

Methods: Conventional X-ray systems and their features were analyzed to define state of the art. A local orthopedic surgeon was consulted and hand surgeries were observed to include user experience within the focus extremity procedures and discuss absolute needed and possible system features. The clinical procedures itself, use of different X-ray systems and observed problems within the workflow were documented. Examples for observed problems during imaging and surgery are:

- Disturbance of workflow due to huge footprint and weight
- Tube-detector-distance limits workspace
- Rotation of X-ray system is not applicable
- Repetition of imaging due to movement or dislocation
- High radiation exposure for the surgeon due to location problems

These findings were integrated in a first conceptual design.

Results: For the proposed FlexScan concept usability, size and cost are essential. Small sized X-ray tubes (Magpro, Moxtek) were combined with a 250mm x

250mm flat panel detector (Xineos 2222HS, TeledynDalsa). The system can be easily fixed and removed using the standard OR table rail. A flexible arm enables a fast positioning and fixation for the image acquisition. An overlay of X-ray cone beam with a light source visualizes the radiation zone.
Conclusion: FlexScan has the potential to improve X-ray-guided interventions on extremities especially for small private surgery centers. To proof the concept a first prototype will be realized and tested with experienced users involved.

ID 22

Conventional sequences for iMRI and their performance

F. Lüsebrink[1,2], U. Kägebein[1,2], O. Speck[1,2]
[1]Otto-von-Guericke University, Forschungscampus STIMULATE, Magdeburg, Germany
[2]Otto-von-Guericke University, Biomedical Magnetic Resonance, Magdeburg, Germany

Introduction: We set up protocols to be used in iMRI with a wide range of contrasts based on Cartesian sampling to allow for real-time reconstruction on common scanner hardware. These include a T_1-weighted GRE, a T_2-weighted HASTE, and a TRUFI with mixed T_1/T_2-weighting. By establishing a performance factor (PF) their performance is assessed.
Methods: For each sequence a fast-, medium-, and slow-paced protocol has been set up, in which the frames per second (FPS) varies between 0.8 and 5. Each measurement consists of three slices and may be aligned either orthogonal or parallel to each other. All sequences include Siemens' IRT functionality allowing for real-time visualization on the scanner and utilization of Siemens' add-ons for interactive needle guidance. One subject has been measured with all protocols on a Skyra 3 T MR scanner using an 8-channel large flex and 8-channel spine coil (all Siemens, Erlangen, Germany). A total of 20 measurements per protocol have been conducted under free breathing with parallel alignment of the slices.
The PF is based on spatial resolution, FPS, signal-to-noise ratio (SNR) and contrast-to-noise ratio (CNR). Each component is multiplied by a normalization factor (NF) and weighting factor (WF). The NFs have been compiled from parameters given in the literature or by our demands on sequences, while the WFs allow adjustments regarding application. SNR has been calculated by dividing the intensity of the liver by a large region of interest outside the body. CNR has been assessed by ratio calculation of SNR in the liver and spleen.
Results: The GRE score a PF of up to 2.6, HASTE of up to 1, and the TRUFI of up to 2.8.
Conclusion: Most protocols perform significantly better or are at least equal compared to protocols described in the literature. The formula for the performance factor can be extended or adjusted easily to rate sequences by own needs, e.g. higher weighting of CNR and less of FPS.

Figure 1

$$PF = \frac{\ell_1}{Resolution} w_1 + \frac{FPS}{\ell_2} w_2 + \frac{SNR}{\ell_3} w_3 + \frac{CNR}{\ell_4} w_4$$

Sequence		Resolution [mm]	FPS	SNR (Liver)	SNR (Spleen)	CNR	PF
TRUFI	Fast	2x2x4	5,0	130	196	1,5	2,8
	Medium	1.5x1.5x4	2,9	100	140	1,4	1,8
	Slow	1x1x4	1,8	63	106	1,7	1,5
GRE	Fast	2x2x4	4,6	67	70	1,0	2,6
	Medium	2x2x4	3,3	99	95	0,9	2
	Slow	2x2x4	2,0	91	100	1,1	1,3
HASTE	Fast	2x2x4	1,3	65	162	2,5	1,0
	Medium	2x2x4	1,0	64	123	2,3	0,9
	Slow	2x2x4	0,8	67	170	2,5	0,9

ID 23

Estimation of femoral artery access location for anatomic deformation correction

K. Breininger[1], M. Pfister[2], G. Koutouzi[3]
M. Kowarschik[2], A. Maier[1]
[1]Friedrich-Alexander-Universität Erlangen-Nürnberg, Pattern Recognition Lab, Erlangen, Germany
[2]Siemens Healthcare GmbH, Forchheim, Germany
[3]Sahlgrenska Academy, University of Gothenburg, Institute of Clinical Science, Department of Radiology, Gothenburg, Sweden

Introduction: Endovascular repair (EVAR) has become the predominant choice for elective treatment of abdominal aortic aneurysms. Fusion of intraoperative fluoroscopic images with segmented vessels from preoperative computed tomography angiography (CTA) can help to reduce the use of nephrotoxic iodinated contrast[1]. Due to anatomic deformations caused by inserted stiff instruments, the segmentation has to be updated to sustain validity[2]. To aid algorithms adjusting for this deformation, we propose a method to automatically estimate the point for arterial access[3] based on the vessel centerline. This vascular point is fixed during the intervention and can thus be used as a boundary condition for correction algorithms.
Materials & methods: Preoperative CTAs from 20 patients undergoing EVAR were collected (Fig. A). Vessel centerlines of left and right common and external iliac and femoral artery were extracted using a semi-automatic segmentation tool. Five CTAs were used for parameter tuning, leaving 30 centerlines for evaluation. Depending on the most ventral centerline point and the curvature proximal to this point, a segment of interest was determined (Fig. B). The final puncture point was defined by analyzing the derivative of the centerline and evaluated against a manually annotated ground truth (GT)(Fig. C).
Results: Mean absolute error was 6.3±4.5mm and below 10mm in 24 out of the 30 vessels (Fig. D). Estimation was less accurate in cases with unusual anatomy, e.g., femoral bifurcation above the femoral head. Maximal error was 18mm.

Conclusion: The proposed method estimates the puncture point with reproducible high accuracy below the vessel diameter, which should be sufficient to aid algorithms correcting for device-induced anatomic deformation.

Disclaimer: The methods and information presented here are based on research and are not commercially available.

References:

1. Kauffmann et al. JVIR 2015
2. Toth et al. MICCAI 2015
3. Bangalore et al. Circulation 2011

Figure 1

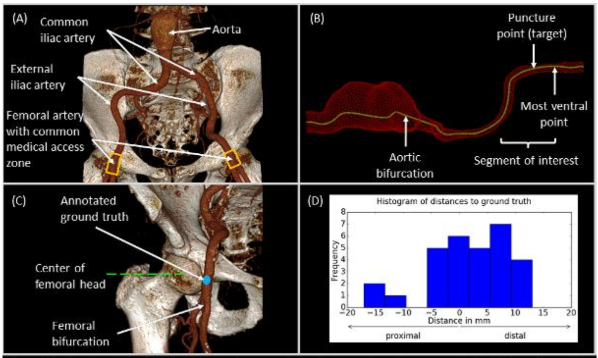

Figure: (A) Vessel anatomy. (B) Lateral view of a segmentation (red: vessel mesh, green: centerline). Depending on the curvature in the region proximal to the most ventral point (defined by min. y-coordinate), a segment of interest is determined, which is smaller for highly curved vessels, and larger for straight vessels. The final puncture point is then defined by the location where the magnitude of the derivative in dorsal-ventral direction falls below a threshold. (C) Ground truth annotation with bone landmark. (D) Distribution of errors proximal/distal to ground truth.
Anatomical images courtesy of Department of Vascular Surgery, Sahlgrenska University Hospital, Gothenburg, Sweden.

ID 24

Patient Access 4.0: Concept for a Suitable Patient Table for Interventional MRI

K. Opfermann[1], L. Junge[1], B. Hensen[2], E. Pannicke[1]
U. Kägebein[3], F. Wacker[2], G. Rose[3]
[1]Otto-von-Guericke Universität Magdeburg, STIMULATE, MR-Tools , Magdeburg, Germany
[2]Medizinische Hochschule Hannover, Hannover, Germany
[3]Otto-von-Guericke Universität Magdeburg, Magdeburg, Germany

Introduction: To carry out a liver ablation with MRI, you have to solve some issues. The MRI-patient-table is not suitable for interventional MRI. For this reason, the table-chassis and the table surface was completely revised.

For executing the liver ablation, the patient will be driven in the MRI-Bore, until the liver is located in the isocenter of the MRI. At that, the feet and a part of the lower leg stay outside of the MRI. For the ablation, the physician has to lean far in above the patient e.g. for the freehand technique [1]. Above all, the chassis of the patient table and the feet of the patient are in the way.

Material & Methods: For this reason, the patient table was newly designed. The chassis was abridged and got only a single support in front of the MRI. The surface of the patient table got a removable gap.

Because there is a generally space problem during the therapeutically intervention inside the MRI, the newly designed surface of the table is about 10 cm lower mounted as usually and generate some additional space for the patient and for the physician (figure 1). Through this, the physician come closer to the patient and will accelerate and improve the workflow of the interventional MRI.

Results: The prototype of the new patient table is constructed from aluminum profiles. We put attention to using only non-ferromagnetic materials like aluminum or certain stainless steel-alloy. Otherwise, it will cause some interferential artefacts during the imaging.

Conclusion: Here is presented a completely new concept for a suitable IMRI patient table, which provide a much better patient access for the physician, will increase the accuracy of the surgery and reduces the MRI-time.

References:

[1] Fischbach, F., et al. Cardiovasc Intervent Radiol (2011) 34:188-192.

Acknowledgement: The work of this paper is funded by the BMBF under grant number '13GW0095A' and '13GW0095C'.

Figure 1

ID 25

Catheter tracking based on catheter curvature and vessel anatomy

J. Strehlow[1], T. Pätz[1], S. Heldmann[2], N. Papenberg[2]
A. Schreiber[1], J. Georgii[1], H. Hahn[1,3]
[1]Fraunhofer, MEVIS, Bremen, Germany
[2]Fraunhofer, MEVIS, Lübeck, Germany
[3]Jacobs University, Bremen, Germany

Introduction: Fiber-optical shape sensing has the potential to change catheter-based interventions. Integrated into a catheter or guidewire, optical fibers with inscribed Fiber Bragg Gratings (FBGs) can reconstruct the shape of an instrument from local strain and curvature measurements. Typical shape reconstruction methods, however, accumulate substantial errors along the length of the fiber, require a fixed reference point on the fiber, and are prone to reconstruction errors due to fiber twisting, hampering the success of this new technology.

Methods: We propose a novel method that uses a-priori vascular information to improve the estimation of the instruments shape. The vascular system is extracted from diagnostic images and the curvature profile along all paths through the vascular system is computed. The local curvature measured along the fiber is used to find a curvature pattern within the vascular system that best explains the measured values. The robustness of the shape estimate is improved by incorporating a history of measured values.

Results: The system is evaluated with a 4-core fiber with 32 FBG sensors per core inserted into a neuro catheter on a transparent vascular phantom. The catheter tip position is visually compared with the estimated position.

The system was able to robustly track the catheter shape in real-time. The catheter tip estimate showed good correlation with the real catheter tip while moving on several paths through the phantom. The estimate was not influenced by higher motion speeds and slight modifications of the phantom shape. Furthermore, the estimate had no noticeable noise.

Conclusions: We could show that the proposed method is suitable for real time catheter tracking and seems to be accurate and precise. After this successful proof of concept, the method will be evaluated quantitatively with data from MR monitoring. It has the potential to emerge to a tracking system that is invariant to patient motion and repositioning.

ID 35

Virtuelle Erhöhung der Röntgensichtbarkeit neurovaskulärer Stents in der Radiographie

T. Hoffmann[1], D. Juhre[2], G. Cattaneo[3], G. Rose[4]
O. Beuing[1]

[1]Otto-von-Guericke University, Institute for Neuroradiology, Magdeburg, Germany

[2]Otto-von-Guericke University, Institute for Mechanics, Magdeburg, Germany

[3]ACANDIS GmbH, Pforzheim, Germany

[4]Otto-von-Guericke University, Institute for Medical Engineering, Magdeburg, Germany

Einleitung: Die Sichtbarkeit lasergeschnittener Stents in der Radiographie wird v.a. durch Werkstoff und Geometrie bestimmt. Wegen der kleinen Dimensionen der Stentstreben sind diese in der Radiographie kaum erkennbar. Oft kann keine sichere Aussage hinsichtlich einer Stentdeformation gemacht werden. Im vorgestellten Verfahren wird die Stentdeformation simuliert, um die Sichtbarkeit in der Radiographie virtuell zu erhöhen.

Material und Methoden: Aus einem präoperativen 3D DSA Datensatz wurde die Zielregion ausgewählt, segmentiert und oberflächenvernetzt. Beim Absetzen des Stents wurden zwei Radiographien aus unterschiedlichen Richtungen erzeugt. Mit Hilfe der Projektionsinformationen wurden daraus die 3D-Markerkoordinaten berechnet. Segmentiertes Gefäß, Markerkoordinaten sowie Stenteigenschaften wurden in die Finite-Elemente-Software importiert und simuliert. Das deformierte Stentmodell wurde voxelisiert und vorwärts projiziert. Nach einer Registrierung, konnte der virtuell deformierte Stent in die Radiographie eingeblendet werden. Die Validierung erfolgte anhand von drei Phantom-Einsatzszenarien.

Ergebnisse: Der Vergleich zwischen realem Modell und Simulation im ersten Fall zeigte ein identisches Deformationsverhalten. Das zweite Phantom beinhaltete eine Stenose. Der Stent zeigte eine gute Übereinstimmung, aber distal Abweichungen. Im dritten Modell wurde das Verhalten bei kleinen Radien überprüft. Das simulierte Ergebnis zeigte ein Knicken, das in vitro nicht gegeben war. Die Sichtbarkeit des Stent-Korpus wurde in allen Fällen erhöht (Abb. 1).

Schlussfolgerung: Der vorgestellte Ansatz zeigt Möglichkeiten zur Erhöhung der Sichtbarkeit von Stents in der Radiographie auf, ohne Änderungen an Geometrie oder Material vorzunehmen. Für das Erreichen einer klinischen Einsatzfähigkeit müssen jedoch verschiedene Faktoren, wie Simulationsdauer und Materialmodell, verbessert werden.

Abb. 1: Initiale (a) und erweitere Radiographie (b).

Figure 1

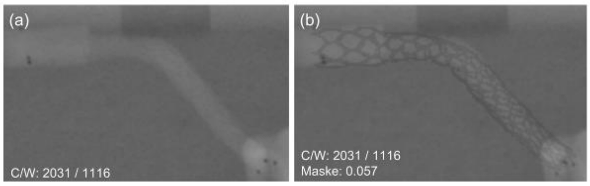

ID 39

Consistency Measure Based Extrapolation of Truncated C-arm CT Data in Cone-Beam Geometry

D. Hellge-Theune[1], R. Frysch[1], G. Rose[1]

[1]Otto-von-Guericke-Universität Magdeburg, Lehrstuhl Medizinische Telematik und Medizintechnik, Magdeburg, Germany

Introduction: A key problem of computed tomography is the reconstruction of tomographic images from incomplete projection data, this is commonly termed truncation. Truncation occurs when the measured region is constrained to not contain the whole patient but only a limited region-of-interest (ROI) leading to image artefacts. A typical strategy to counter these is the extrapolation of the measured region.

Materials & Methods: A new extrapolation algorithm was developed, utilizing a-priori information about valid cone-beam CT projections. It uses an ellipsoid as the extrapolation model whose parameters are optimized by minimizing a novel consistency metric, which is derived from redundancies between projections of the same object from different angles, arising from the fundamental relation of Grangeat. In the case of truncation, certain conserved quantities are increasingly mismatching, yielding a consistency measure suited for truncation problems.

Results: The performance of the algorithm was tested using truncated projections from several software-phantoms where the ROI is entirely embedded in the patient. An increase in the effectively usable ROI is observed at the cost of slightly decreased contrast leading to an overall improved image quality. This improvement is also reflected in established image quality metrics. For certain artificial phantoms, however, the algorithm has shown to be not very robust, yet.

Conclusion: It was shown, that Grangeat-based consistency metrics which were previously used for motion-compensation etc. are also suited as a basis for the extrapolation of truncated projections. Furthermore, great improvements to the algorithm regarding speed and robustness can be expected upon more efficient implementation.

This work was conducted within the International Graduate School MEMoRIAL at OVGU Magdeburg, supported by the ESF (project no. ZS/2016/08/80646). This work is partly funded by the German BMBF within the FC STIMULATE (13GW0095A).

ID 52

Beam harening correction using Grangeat-based consisteny measure

S. Abdurahman[1], R. Frysch[2], R. Bismark[3]
O. Beuing[3], G. Rose[3]

[1]Otto-von-Guericke-Universität Magdeburg, IMT/INKA, Magdeburg, Germany

[2]Otto-von-Guericke-Universität Magdeburg, Institut für Medizintechnik, Magdeburg, Germany

[3]Otto-von-Guericke Universität, STIMULATE, Magdeburg, Germany

Introduction: The polychromatic X-ray spectrum and energy-dependent attenuation coefficient of materials cause beam hardening artifacts in CT reconstructed volumes. These artifacts appear as cupping, streak and spill-over artifacts and reduce the contrast resolution. CT scanners employ water correction to transform polychromatic attenuation to monochromatic attenuation using a polynomial model. Polynomial coefficients are computed during calibration or using prior knowledge like X-ray and material attenuation spectra. For C-arm CT, water correction is not sufficient to correct bone induced beam hardening artifacts.

Materials & methods: We present a novel method to correct beam hardening artifacts by enforcing cone beam consistency conditions on the projection data. We used consistency conditions derived from Grangeat's fundamental relation between cone beam projections and 3D Radon transform. The optimal polynomial coefficients for artifact reduction are iteratively estimated by minimizing the inconsistency between a pair of cone beam projections.

Results: The results from simulated and clinical datasets show that the proposed correction considerably reduces cupping, streak and spill-over artifacts (see Fig. 1).

Conclusion: The novel Grangeat-based consistency measured can be used to reduce beam hardening artifacts in clinical C-arm CT without prior knowledge and increased computational complexity.

This work is partly funded by the Federal Ministry of Education and Research within the Forschungscampus STIMULATE under grant numbers '13GW0095A' and '03IPT7100X' (INKA).

Figure 1: Reduction of spill over artifacts due to beam hardening: (left) Before correction; (middle) after water correction from the scanner; (right) after consistency based beam hardening correction

Figure 1

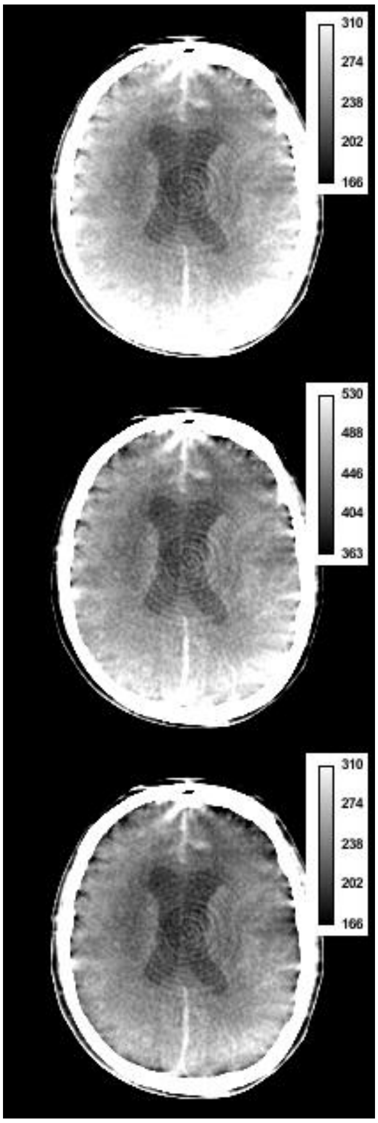

ID 53

Hip Implant Wear Measurement in X-Ray Images using 2D-3D-Registration

S. Klebingat[1], G. Rose[1]

[1] Otto-von-Guericke Universität Magdeburg, Magdeburg, Germany

Introduction: There exist several approaches measuring hip implant wear in anterior-posterior x-ray images of the pelvis [1, 2]. We introduce a 2D-3D-registration based approach giving precise results in a micrometer range in a first in-vitro study requiring minimal user interaction.

Materials & methods: An experimental setup holding a hip implant cup and allowing the precise movement of a hip stem with an applied head in two orthogonal directions was put in-plane inside a x-ray device (see Figure 1). The stem/head were precisely moved within both directions of the plane. CAD voxel models are used for 2D-3D-registering the implants calculating the changing distances of their centers.

Results: The delta of the center positions of 25 unique combinations of movement in both directions could be calculated with a mean error of less than 5 micrometers. The results are reproducible in a way that the user does not have to set any parameters or marks required for the registration.

Conclusion: Within certain restrictions this methods shows very promising initial results for precise hip wear measurement. Future work shall investigate how especially out-of-plane movements can be handled.

The study was partially funded by the Central Innovation Programme of the German Federal Ministry for Economic Affairs and Energy [project number KF3357302KJ4].

References

[1] Burckhardt et al.: Measuring orthopedic implant wear on standard radiographs with a precision in the 10 µm-range, Medical Image Analysis 10 (2006)

[2] J. Martell, S. Berdia: Determination of Polyethylene Wear in Total Hip Replacements with Use of Digital Radiographs, The Journal of Bone and Joint Surgery (1997)

Figure 1: Device containing the hip implant components and a resulting x-ray image

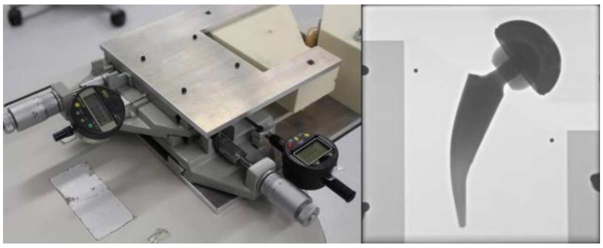

Robotic

ID 08

Patientenindividuelle und präzise Behandlung von Wirbelsäulenmetastasen

J. Hettig[1], M. Hanses[2], S. Adler[2], C. Rieder[3], M. Becker[4] M. Skalej[4], N. Elkmann[2], C. Hansen[1]

[1]STIMULATE, Magdeburg, Germany

[2]Fraunhofer IFF, Magdeburg, Germany

[3]Fraunhofer MEVIS, Bremen, Germany

[4]Institut für Neuroradiologie, Magdeburg, Germany

Die Patientenindividuelle Planung zur Behandlung von Wirbelsäulenmetastasen bietet einen hohen Detailgrad und somit die Grundlage für eine sichere und genaue Intervention. Ziel ist es, den Eintrittspfad der Ablationsnadel zu bestimmen, sowie eine Vorhersage über die Nekrosezone zu treffen. Für eine präzise Durchführung wird ein chirurgischer Assistenzroboter verwendet. Dadurch soll das Verletzungsrisiko von Risikostrukturen, sowie die Strahlenbelastung für Patient und Arzt reduziert werden. Die Planung basiert auf einem präoperativen MRT Datensatz, welcher mit der Software MeVis SAFIR verarbeitet wird. Im ersten Schritt werden anatomische Strukturen semi-automatisch segmentiert. Anschließend wird die Position der Ablationsnadel geplant und eine Simulation der Ablationszone durchgeführt. Im Anschluss an die Planung, werden die Positionsinformationen der Ablationsnadel an den Assistenzroboter übertragen. Nach einer intraoperativen Registrierung, führt der Roboter die Ablationsnadel zur geplanten Einstichstelle. Im Anschluss kann der Chirurg die Ablationsnadel in Kooperation mit dem Assistenzroboter zu der geplanten Zielposition führen und die Ablation kann entsprechend der Planung durchgeführt werden. Sollte es bei der Platzierung zu Abweichungen kommen, wäre eine Aktualisierung der Planung notwendig. Dazu wird die Nadelposition zurück an die Planungssoftware übertragen, woraufhin eine neue Simulation durchgeführt wird. Die Evaluierung wurde an einem Phantom unter realen Bedingungen durchgeführt. Es konnte gezeigt werden, dass eine erhöhte Präzision und verringerte Strahlenlast mit einem nur minimalen Mehraufwand gegenüber einer konventionellen Intervention erreicht wird. Der beschriebene Arbeitsablauf ermöglicht eine präzise Planung, sowie Durchführung bei der Behandlung von Wirbelsäulenmetastasen. Zusätzlich besteht die Möglichkeit der echtzeitfähigen Anpassungen des Interventionsplanes und einer anschließenden Korrektur. Förderkennzeichen: 13GW0095A und 13GW0095B.

ID 11

Accuracy of registration between a Robotic System and a Medical Imaging System

A. Gulhar[1], P. Mewes[2], G. Rose[3]
[1]Siemens Healthcare GmbH, Diagnostic Imaging, X-ray Products, Forchheim, Germany
[2]Siemens Healthcare GmbH, Advanced Therapies, Surgery, Forchheim, Germany
[3]Otto-von-Guericke University, Magdeburg, Medizinische Telematik und Medizintechnik, Magdeburg, Germany

The presence of robots not only for industrial production but also in operative rooms is increasing rapidly with the advancement of technology and time. The combination of medical imaging modalities with robots enables them to be guided to anatomical structures in the human body provided the robot is registered to the medical imaging system. In this paper, we evaluate the accuracy of 6 degrees of freedom registration of a robotic system to a medical imaging system without the use of any tracking device. The registration is realized by a series of landmark transformations whose positions are already known in the coordinate system of the imaging system. Multiple factors affect the accuracy of registration between a robotic system and a medical imaging system, with accuracy of pose (AP) of the robot being one of the primary factors. This factor is investigated in this paper and is thereafter incorporated in the final registration accuracy. The AP of the robotic system is evaluated using a tracking system which results in a mean deviation of 0.24±0.07 mm, 0.21±0.08 mm, 0.25±0.11 mm, 0.35±0.15 mm from the desired position when the robot is driven by a relative distance of 10 cm, 20 cm, 30 cm, 40 cm respectively. After incorporating the AP in registration accuracy of the robotic system with a medical imaging system, a mean norm translation error of 11.88±0.40 mm and a mean rotational error of 1.71 degrees are obtained when compared to an X-ray based ground truth registration. Considering the accuracy, reliability, stability and robustness of this registration approach, it may not necessarily serve as the primary registration between the robot and the imaging system but could be useful in clinical environment as a redundant / secondary registration to prevent unforeseen accidents. Also, this approach is useful as it does not expose the patient to unwanted X-ray radiation in case the registration needs to be repeated many times during an intervention.

ID 14

An image-based robotic needle guidance system for interventional radiology

T. Pätz[1], A. Rothfuss[2]
[1]Fraunhofer MEVIS, Bremen, Germany
[2]Fraunhofer IPA, Projektgruppe für die Automatisierung in der Medizin und Biotechnologie PAMB, Mannheim, Germany

Intro: We present a pre-clinical robotic guidance system with a dedicated image-based control software to support needle-based interventions in the angio suite. We also present first precision results for needle placement.
Methods: The system consists of a Kuka LBR robot, equipped with a control software with OpenIGTLink interface and an image-based calibration and target planning software based on MeVisLab. The robot can hold either a calibration tool, containing 4 spheres with known geometry for coordinate system alignment of the imaging device and the robot or a needle-guide that prescribes the needle trajectory and supports multi-needle-placement. For needle placement, the robot places the needle guide on the patient skin to determine the needle entry point. The calibration and targeting software provides automatic calibration tool detection, image segmentation, registration, virtual needle placement, and ablation simulation.
For the precision analysis we used a 15cm 16G needle that has been placed at n=13 target positions. For all positions, we compared planned and reached needle path in air and a gelatin phantom.
Results: The robotic guidance system had an overall angular deviation between planned and reached position that is below 1° (range 0.50° to 1.37°), and an overall deviation of the shaft resp. skin entry point of 1.4mm (range 0.69mm to 2.41mm). Reproducibility of the needle path between air and gelatin was far better than overall system precision leaving potential for further system improvements. Time required for robot motion to target, needle insertion, 3D scan, needle removal, and robot motion to rest position was less than two minutes for this technical setup.
Conclusion: The analyzed system has a better angle and shaft precision as reported for comparative systems. It is easy to use and fast. The system has potential to serve as a fully integrated biopsy and therapeutic needle intervention system in head and neck, pulmonary, and abdominal areas.

Figure 1

ID 43

Towards collision detection in modern hospital operating rooms using Deep Learning methods

P. Schülein[1], M. Vetter[1]

[1]Mannheim University of Applied Sciences, Institut für eingebettete Systeme und Medizintechnik (ESM), Mannheim, Germany

Question: Hospital operation rooms for minimally invasive therapies, often contain robots for x-ray imaging. When working with them, collisions between health professionals or medical devices may occur. These collisions happen, when the robot position or orientation is changed. Collisions should be predicted and avoided.

Methods: The detection of objects can be achieved by modern machine learning techniques like Deep Learning utilizing images taken by ToF cameras. Object detection with color imaging devices is already well-established [1]. We believe that the additional depth information will stabilize the system in occluded scenarios like the operating room. For detecting the health professionals or the patient, the skeleton of them, can be determined by methods mentioned in [2]. In areas where collisions are likely to happen, additional sensors like capacitive distance sensors or ToF cameras increase security.

Results: The suitability of those sensors in a clinical environment was examined in a feasibility study inside an experimental operating room. For skeleton detection, we use [3]. However, machine learning methods, for more robust detection, will be used in future work, Fig. 1. Object detection is carried out by classical tracking methods which will also be exchanged with Deep Learning methods.

Conclusion: Deep Learning methods proved to be superior in object detection and classification [1]. In operating rooms with robots, the detection of possible collisions is essential. By combining those methods with additional sensors, even small objects can be detected and thus collisions are avoided.

List of Figures: Fig. 1: Exemplary scene with detected objects and their respective bounding boxes.

References:

[1]: K.He et al. "Deep Residual Learning for Image Recognition" https://arxiv.org/abs/1512.03385

[2]: E. Insafutdinov et al. "DeeperCut" https://arxiv.org/abs/1605.03170

[3]: M. Rietzler et al. "FusionKit", In Proc. of EICS 2016, 8th ACM SIGCHI

Figure 1

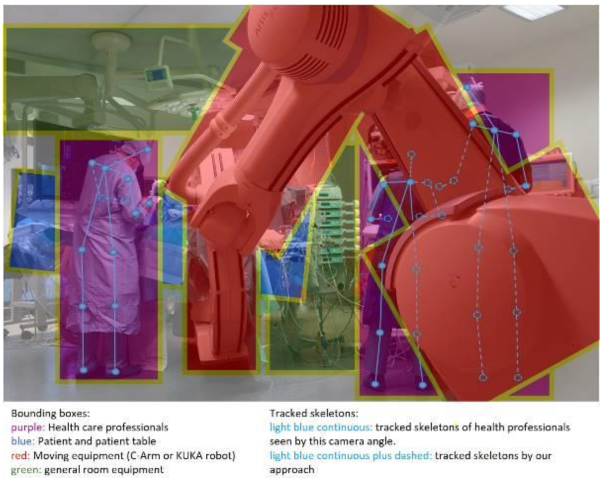

Spine

ID 26

Assessing suitable MRI sequences for subsequent spinal metastasis segmentation

G. Hille[1], S. Saalfeld[1], S. Serowy[2], K. Tönnies[1]

[1]University of Magdeburg, Department of Simulation and Graphics, Magdeburg, Germany

[2]University Hospital of Magdeburg, Department of Neuroradiology, Magdeburg, Germany

Owing to the fact that cancerous diseases will be more frequently than ever and metastases located in the spine predominate. Furthermore, the segmentation of vertebral metastases is a pivotal step towards therapy planning and RFA simulation to assign state-dependent tissue parameters. Though, massive obstacles for metastasis segmentation in spine MRI are poor image contours between pathologic and healthy tissues, variable signal behavior of the metastases and deformations due to the metastatic bone alteration. The usage of images, where a sufficiently good differentiation between metastasis and surrounding tissue is possible, constitutes a critical requirement for successful segmentation procedures.

The aim of our work is to find the most suitable MRI sequences or combination of sequences (difference images) of each patient for subsequent spinal metastasis segmentation procedures. Thus our method will determine images with preferably high image contrast between metastasis and both healthy vertebra and disk image signals. Therefore, we searched for

images with high histogram dissimilarity within joint cumulative histograms of all three tissue types. As a dissimilarity measure we used correlation distances. To evaluate our method, we matched the produced results of 10 patients, each with up to 4 MRI sequences, with a ranking of a segmentation expert. Spearman"s ranking coefficient was used to match the algorithmically preferred sequences with those of the field expert.
Our method showed reasonable results for choosing suitable MRI sequences out of bunch of diagnostically acquired images and their combinations. This pre-processing step could speed up clinical segmentation procedures due to omitting the time-consuming manual initialization of choosing suitable images.

ID 28

Magnetic tracking using integrated sensor and isocentric orthogonal generator.

D. Terlinden[1]
[1]metraTec GmbH, R&D, Magdeburg, Germany

Introduction: Tracking of an RFA probe during minimally invasive ablation of metastases next to risk structures like the spine is essential to correlate the real instruments position with imaging prior to intervention. Commonly used CT or X-ray imaging are based on ionizing radiation and optical tracking systems only work sufficiently under line-of-sight conditions. Thus magnetic tracking with supporting inertial navigation is preferable avoiding aforementioned disadvantages as discussed in this work.
Materials & methods: To prove a novel set of equations to calculate the instrument's position and attitude directly, a test setup was designed. This contains a set of three isocentric and orthogonal excitation coils driven by a pattern based, current controlled DC driver circuit and an integrated sensor, that incorporates a 3-axes AMR sensor for detecting the magnetic flux density as well as a gyroscope and an accelerometer. Using time-domain multiplexing, the nine elements of the magnetic transmission matrix are determined and passed to the direct tracking algorithm. To take reference measurements, optical fiducial marks have been attached to both generator and sensor and a software interface for NDI Polaris tracking system was developed.
Results: A novel mathematic approach to determine the sensor's position and attitude with respect to the generator turned out to be suitable for tracking medical instruments. No non-linear optimization is necessary in this approach. Due to the excitation principle field distortion by non-ferrous metal is negligible. The geometry of the excitation coils has been optimized to increase the accuracy.
Conclusion: A prototypical magnetic tracking system was built using three orthogonal excitation coils and an integrated sensor with IMU capability. The novel direct calculation of position and attitude has been successfully demonstrated.

Stroke

ID 36

Entwurf, Konstruktion und Validierung eines Versuchsstandes zur Simulation des Temperaturverhaltens bei intraarterieller Hypothermie im menschlichen Gehirn

T. Hoffmann[1], M. Breitkopf[1], M. Kalmar[2], F. Klink[2]
G. Cattaneo[3], O. Beuing[1]
[1]Otto-von-Guericke University, Institute for Neuroradiology, Magdeburg, Germany
[2]Otto-von-Guericke University, Institute for Mechanical Engineering, Magdeburg, Germany
[3]ACANDIS GmbH, Pforzheim, Germany

Einleitung: Durch lokale Zellkühlung kann das Behandlungsfenster zur Therapie von Gewebeschäden beim Schlaganfall vergrößert werden. Als vielversprechende nicht-invasive Methode zur Überwachung der lokalen Kühlvorgänge im Gehirn gilt die Magnet-Resonanz-Spektroskopie (MRS). Das genannte Verfahren basiert auf der temperaturabhängigen Verschiebung der Protonen-Resonanzfrequenz unterschiedlicher Materialien. Ziel der Untersuchung war es, einen MRS-kompatiblen Versuchsaufbau eines in-vitro Gehirnmodells mit Gefäßbifurkation und der Möglichkeit zur Schlaganfallsimulation zu etablieren, der die Wärmeleiteigenschaften des menschlichen Gehirns nachbildet.
Material und Methoden: Die temperaturbestimmenden Eigenschaften des Gehirns beim Schlaganfall wurden analysiert. Die daraus für den Versuchsstand abgeleiteten Anforderungen beinhalten u.a. die Notwendigkeit der konstanten Temperierung des Gehirnmodells von außen sowie die Möglichkeit der Durchströmung des Modells mit Fluiden unterschiedlicher Temperaturen und die Einbringung eines gezielten Gefäßverschlusses. Ein Hydrogelmaterial mit ähnlicher Wärmekapazität sowie Leitfähigkeit zum realen Gehirngewebe wurde bestimmt. Die Validierung des Versuchsstandes erfolgte durch MRS-Messungen am Modell mit ungehinderter Durchströmung und partiell verschlossenem System.
Ergebnisse: Es wurde ein Versuchsstand konzipiert, konstruiert, gefertigt und mittels MRS getestet. Das genutzte Hydrogelmaterial zeigte ein homogenes Signalverhalten. Die MRS-Temperaturmessung konnte durch optische Temperatursensoren sowohl für den simulierten Schlaganfall als auch für den freien Gefäßdurchfluss bestätigt werden.
Schlussfolgerung: Der umgesetzte Versuchsstand ermöglicht es im vereinfachten Modell einer

Gefäßbifurkation einen Schlaganfall zu simulieren und die Temperaturänderung im Gehirnphantom mittels MRS und optischer Temperatursensorik zu überprüfen. Außerdem ist die Integration von Gehirnmodellen mit höherer Komplexität möglich.

ID 40

Improvement of BMI control by Detecting Errors from EEG and MEG Recordings

C. Reichert[1], N. Heinze[1], T. Pfeiffer[2], H. Hinrichs[1,3,4,5]

[1]Leibniz Institute for Neurobiology, Dept. of Behavioral Neurology, Magdeburg, Germany

[2]Otto-von-Guericke University, Institute for Medical Engineering, Magdeburg, Germany

[3]Otto-von-Guericke University, Dept. of Neurology, Magdeburg, Germany

[4]Center for Behavioral Brain Sciences (CBBS), Magdeburg, Germany

[5]German Center for Neurodegenerative Diseases (DZNE), Magdeburg, Germany

Introduction: Brain-Machine Interfaces (BMIs) are intended to regain communication and mobility in severely disabled persons. Perspectively, BMIs can be used to rehabilitate stroke patients or to control prosthetic and robotic devices. However, noninvasive BMIs suffer from low signal quality, resulting in erroneous commands. Such errors could be avoided by detecting error potentials (ErrPs) in the brain, evoked after the perception of erroneous feedback. Here we investigate the ability to improve BMI control by detecting perceived errors in EEG and MEG.

Methods: We decoded the presence of ErrPs in simultaneously recorded EEG and MEG from 19 subjects participating in a BMI experiment with a balanced number of correct and incorrect feedback. Using spatial filtering and SVM classification, we determined the probability of detecting an ErrP. Finally, we evaluated the potential benefit of ErrP detection to prevent erroneous feedback in a BMI using probability theory.

Results: The components extracted by the data-driven spatial filter showed a positive deflection between 200 and 500 ms after feedback presentation, mainly driving the ErrP decoding. On average, the correctness of perceived feedback could be decoded with an accuracy of 71.9% using EEG (MEG: 72.7%, nonsignificant improvement). This error detection could reduce the error rate of a BMI by rejecting potentially false commands. However, the error rate of the ErrP classification inevitably introduces accidental rejection of correct feedback which counteracts these benefits.

Conclusion: EEG and MEG are comparably suitable to detect a user's perception of erroneous feedback from brain activity recordings. The achieved prediction rate is in accordance with other approaches reported in the literature, only focusing EEG. Although the approach can reduce the number of incorrect BMI commands, it concurrently rejects correct commands. We conclude that ErrP detection is only advantageous if error detection rates exceed the accuracy of the feedback generating BMI.

ID 47

Robust Computation of Perfusion Maps for Spatiotemporal Model-based CT Reconstructions

Sebastian Bannasch, Gerald Warnecke and Georg Rose

S. Bannasch[1], G. Warnecke[2], G. Rose[1]

[1]Institute of Medical Engineering, Magdeburg, Germany

[2]Institute of Analysis and Numerics, Mathematik, Magdeburg, Germany

Introduction: In case of 4D CT, the dynamics of bolus distribution is quantified by 3D perfusion maps (PMs) for stroke diagnostics. However, the calculation of certain PMs, e.g. the CBF, is numerically unstable.

Materials & methods: For the application of model-based reconstructions (MBPR), the contrast time attenuation curves (TACs) are described by a superposition of temporal functions. The properties of these basis functions, such as smoothness, are transferred to the perfusion mapping algorithm based on [1].

Results: By means of reconstructed TACs of simulated C-Arm data, we calculated the cerebral blood flow for illustration. In the figure, we see f. l. t. r. the ground truth, a common deconvolution and the model-based approach. The model-based approach obviously improves image quality.

Conclusion: We provide a robust computation of PMs for MBPR such that the unstable deconvolution approach can be avoided. This improves the image quality and can increase the accuracy of stroke diagnostics.

Acknowledgements: The work of this paper is partly funded by the Federal Ministry of Education and Research within the Forschungscampus *STIMULATE* under grant number 13GW0095A. Furthermore, this work was in part conducted within the context of the *International Graduate School MEMoRIAL* at Otto-von-Guericke University (OVGU) Magdeburg, Germany, kindly supported by the *European Structural and Investment Funds* (ESF) under the programme "*Sachsen-Anhalt WISSENSCHAFT Internationalisierung*" (project no. ZS/2016/08/80646).

[1] Fieselmann, Kowarschik, Ganguly, Hornegger, Fahrig. Deconvolution-based CT and MR Brain Perfusion Measurement: Theoretical Model Revisited and Practical Implementation Details

Figure 1

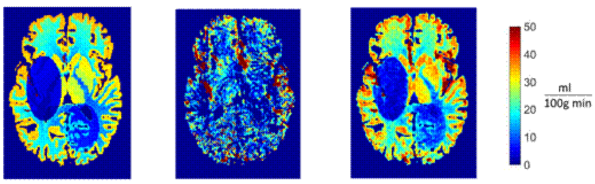

ID 48

Iterative Algebraic Reconstruction of Truncated Projections

R. Frysch[1], G. Rose[1]

[1]Otto-von-Guericke-Universität Magdeburg, Institut für Medizintechnik, Magdeburg, Germany

Introduction: Image reconstruction of truncated projection data is a common issue in clinical computed tomography or interventional C-arm CT. In a recent study, we showed that a certain weighting technique (DWART [1]) improves image quality in iterative reconstructions.

Materials & methods: Our algebraic technique is conceivable as a weighting dependent on the accumulated X-ray density of the scan within a voxel, which is known from algorithms like SIRT/SART [3]. It is compared to a known analytical method with a specialized filtering scheme for truncated projections (ATRACT [2]).

Results: We could verify that the propose method leads to superior reconstruction accuracy compared to the analytical method (see Figure 1). It reduces the inhomogeneity inside the region of interest as well as the bright circular artifact at the edge. Fig.1: F.l.t.r. - original phantom, ATRACT and DWART. The first row shows the reconstructions of a Shepp-Logan phantom and the second a slice of a realistic anatomical software phantom. Each row depicts the same window width, whereby the center of the ATRACT result in the second row is offset corrected.

Conclusion: A higher computational effort for the iterative reconstruction approach using the DWART algorithm compared to dedicated analytical methods could be acceptable for certain clinical applications, since it can distinctly improve image quality in highly truncated imaging scenarios.

This work is partly funded by the Federal Ministry of Education and Research (BMBF) within the Forschungscampus STIMULATE under grant number '13GW0095A'.

References:

[1] R. Frysch, R. Bismark, A. Maier, G. Rose: Ray-Density Weighted Algebraic Reconstruction for Volume-of-Interest CT, Fully3D 2017
[2] F. Dennerlein, A. Maier: Region-of-interest reconstruction on medical C-arms with the ATRACT algorithm, SPIE 2012
[3] P. Gilbert: Iterative methods for the three-dimensional reconstruction of an object from projections, Journal of Theoretical Biology, 1972

Figure 1